MINIMIZING OPTIMAL CO_2 FEED TO ALGAL CULTURES UTILIZING MICROFLUIDIC DEVICES GENERATING MICRON-SIZED BUBBLES

by

Jordan J. Baker

A thesis submitted to Johns Hopkins University in conformity with the requirements for the degree of Master of Science in Engineering

Baltimore, Maryland

June, 2015

Abstract

With amplified environmental damage caused by increased carbon dioxide levels in the atmosphere and the rising cost of energy, algae offer solutions to both world issues as well as many others. Microalgae naturally produce lipids (biofuels), carotenoids (antioxidant health supplements/nutraceuticals), proteins (pharmaceuticals), as well as many other products while removing carbon dioxide from the atmosphere through photosynthesis.

The optimal carbon dioxide feed conditions were tested in a microalgae strain, *Chlorella vulgaris*, to fix the largest amount of carbon dioxide, provide the fastest growth, and produce the greatest concentration of desired components. Feeding 10% carbon dioxide led to the highest growth rate and had the greatest productivity of biomass, total protein, lipids, and lutein (carotenoid) in terms of time, volume of reactor, and cost.

In addition to finding the optimal carbon dioxide feed concentrations, a microfluidic device (channels <70 μm) was utilized to create micro-scale bubbles to significantly increase mass transfer at low flow rates. The convergence of one gas and two liquid channels at a Y-junction generated bubbles via cyclic changes in pressure. At low flow rates, the bubbles had an average diameter of 114 μm, corresponding to a volumetric mass transfer rate (K_La) of 1.43 hr^{-1}. Normalized K_La values demonstrated that the microbubbler had a 100-fold increase in mass transfer per flow rate compared to four other commonly used bubblers. The calculated percentage of oxygen transferred was 90%, which was consistent with a separate off-gas analysis. The improved mass transfer was also tested in an algae bioreactor in which the microbubbler culture absorbed approximately 90% of the CO_2 feed compared to 2% in the culture with an alternative

needle bubbling method. The microbubbler yielded a cell density only 82% of the cell density for the needle tip, but with an 800 fold lower flow rate (0.5mL/min versus 400 mL/min) and a 700 fold higher ratio of biomass to fed gas. The application of the microfluidics may transform interfacial processing in order to increase efficiencies, minimize gas feeding, and provide for more sustainable multiphase processes.

Finding the ideal carbon dioxide feed of 10% CO_2 to *vulgaris* cultures allows for fast, efficient production of biofuels, nutraceuticals, pharmaceuticals, and many other products while helping the environment by fixing carbon dioxide. Through an exceptional improvement in mass transfer from a gas to a liquid, the microfluidic bubbler improved the carbon dioxide fixation and growth rate for microalgae, decreasing costs for bioreactors. This microbubbler can also be used to improve gas sequestration, bioreactors, chemical reactions, and many other industrial processes.

Readers: Dr. Michael J. Betenbaugh (Faculty Advisor) and Dr. Marc Donohue

Acknowledgements

I would like to greatly thank Dr. Michael Betenbaugh for allowing me numerous opportunities to perform research and learn various topics and techniques in his lab. I would also like to thank the other graduate students Coral Fung Shek, Chien-Ting Li, Amanda Tang, Jimmy Kirsh, Saratram Gopalakrishnan, Andrew Chung, Joseph Priola, and Kelly Heffner who have helped me perform my work. Kathleen Rand, Nathan Li, Siswo Hartoyo, Nick Kruyer, and Kate Hobble were all undergraduates who have helped me tremendously with this work. Dr. Julian Rosenberg, Dr. Pavlo Bohutskyi, Dr. Geng Yu, Dr. Yue Zhang, Dr. Maciek Antoniewicz, and Dr. George Oyler all provided me with critical guidance and teachings with my work. I would also like to thank my friends and family, especially my parents, who have supported and helped me throughout this process and deserve all of the credit.

Table of Contents

Abstract ii

Acknowledgements iv

List of Tables vii

List of Figures viii

Chapter 1: Introduction 1

Chapter 2: Materials and Methods 5

2.1 Strain Selection and Culture Conditions 5

2.1.1 Strain Selection 5

2.1.2 Culture Media 5

2.1.3 Culture Conditions 5

2.2 Cell Growth and Size Analysis 6

2.2.1 Cell Density 6

2.2.2 Cell Size 7

2.3 Intracellular Component Analysis 7

2.3.1 Lipid Analysis 7

2.3.2 Protein Analysis 7

2.3.3 Pigment Analysis 7

2.4 Microfluidic Bubbler Construction and Operation 9

2.4.1 Fabrication 9

2.4.2 Operation 11

2.4.3 Comparative Bubbling Equipment 11

2.5 K_La Determination 12

Chapter 3: Identifying Optimal CO_2 Feed 15

3.1 Introduction 15

3.2 Correlation Between Cell Density and Optical Density 17
3.3 Growth Under Varying CO_2 Conditions 19
3.4 Cellular Component Differences in Different CO_2 Conditions 22
3.5 Light Versus Dark Cycle Variations 26
3.6 Economic Analysis 30
3.7 Carbon Dioxide Feed Conclusions 31
Chapter 4: Microfluidic Bubbling Device 34
4.1 Gas Transfer 34
4.2 Microfluidic Device Design 39
4.3 Bubble Sizes 41
4.4 K_La Determination 44
4.5 Fraction Transferred 46
4.6 Frequency Analysis 50
4.7 Bubbler Test in Culture 51
4.8 Economic Analysis 53
4.9 Microbubbler Conclusions 55
Chapter 5: Summary and Future Work 60
5.1 Summary 60
5.2 Future Work 62
References 65
Biographical Statement 68

List of Tables

1. Growth rates for *Chlorella vulgaris* under varying carbon dioxide feeds……21

2. Initial and final culture pHs under varying carbon dioxide conditions…… 22

3. Economic analysis of carbon dioxide feed concentrations…….……..…….. 31

4. Flow and growth rates with CO_2 concentration in headspace and CO_2 fed per biomass for the microbubbler compared to needle bubbling.…….…...…. 53

5. Economic analysis of the microbubbler system against other methods of bubbling.... 54

List of Figures

1. HPLC DAD graph for pigment analysis…… 9

2. Macroscopic view of microfluidic bubbler…….…….…….… 10

3. Microfluidic bubbler channel and mask design…… 10

4. Dissolved oxygen concentration over time for the calculation of K_La …… 13

5. Plot of the natural log of the saturation dissolved oxygen concentration minus the dissolved oxygen levels for the area of interest ……... 14

6. Cell density dependence on optical density……..…… 19

7. Growth curve for *Chlorella vulgaris* under varying carbon dioxide feeds..…….…… 20

8. Dry cell weight, biomass productivity, cell weight, protein concentration, and lipid content for varying carbon dioxide concentrations……..…… 23

9. Chlorophyll and lutein content for all carbon dioxide feeds…….…… 25

10. Carbon dioxide reactions in aqueous media…….…….……. 26

11. Dry cell weight, individual cell weight, protein concentration, and lipid content for night and day cycles…….…….…… 27

12. Cell size distribution of light and dark cycles for the 12.5% reactor..…… 28

13. Chlorophyll and lutein concentration in night and day cycles…… 29

14. Gas-liquid phase boundary…….…… 36

15. Design and size specification of the Y-junction of the microfluidic device ……..… 40

16. Bubbles formed in liquid media…….…….…… 42

17. Size distribution of bubbles created by the microfluidic bubbler...…… 42

18. Bubble size dependence on flow rate for all devices……...… 44

19. K_La and normalized K_La values for the microbubbler and other bubbling methods.. 45

20. K_La dependence on flow rate for all devices.…….…… 46

21. Fraction of oxygen transferred dependence on flow rate for all systems…….…… 47

22. Oxygen gas concentration in the head space above the K_La testing……..…… 49

23. Bubble frequency dependence on height of liquid for a range of flow rates..…… 50

24. Growth curve for *Chlorella vulgaris* comparing the microbubbler to needle tip for gas feed…….…….…… 52

Chapter 1

Introduction

One of the most influential and harrowing problems of the world, climate change, stems from increased concentrations of greenhouse gases in the atmosphere. Greenhouse gases include carbon dioxide (CO_2), methane, ozone, nitrous oxide, and others that all work to trap radiation in the atmosphere, raising the temperature of the planet. The gas that has had the biggest change in recent history is carbon dioxide, rising from 319 parts per million (ppm) in 1960 to approximately 400 ppm today (Dlugokencky & Tans, 2015).

Even though approximately half of current carbon dioxide emissions are absorbed by natural land and ocean sinks, the decrease in future absorption, due to deforestation and other industries, coupled with rising emissions, will lead to further increased carbon dioxide levels (Ballantyne et al., 2012). Therefore, other possible sinks or uses for carbon dioxide must be utilized in order to keep carbon dioxide levels within safe concentrations for the environment.

Photosynthetic organisms, such as algae, that uptake carbon dioxide naturally, provide a countermeasure to the rising carbon dioxide levels. Algae farms sequester several times more carbon dioxide per unit area than other photosynthetic organisms, such as trees or crops, making them an efficient choice for fixing carbon dioxide (Chelf et al., 1992). However, all plants, including algae, only mitigate approximately 3-6% of the carbon dioxide from fossil fuel emissions (Chinnasamy et al., 2009).

Microalgae can help control the carbon dioxide levels in the atmosphere two ways: a preventative method and a restorative treatment. Instead of releasing the off gases, or flue gases, into the atmosphere, large industrial plants can use these gases, rich in carbon dioxide from combustion reactions, as a feed to microalgae cultures. This way, the microalgae can absorb and utilize the carbon dioxide to increase growth rates, lowering the concentration of carbon dioxide in the flue gas before being emitted into the atmosphere.

The other way microalgae cultures help the environment is through a restorative treatment, which acts to lower the concentration of carbon dioxide already in the atmosphere. This would occur with large algae farms using atmospheric air as a carbon dioxide source. Microalgae farming requires less land to absorb equivalent amounts of carbon dioxide than other photosynthetic organisms, plants, and crops; however, they require a larger amount of water than the other plants and food crops (Chinnasamy et al., 2009).

In either case, an improved mass transfer of carbon dioxide from the gas phase to the liquid improves carbon dioxide transfer and mitigation. The mass transfer rate can be increased by decreasing the bubble size of the gas flowing into the liquid. If the mass transfer from the gas to the liquid increases, the algae will have a faster growth rate due to the higher efficiency of the transfer.

Having an increased mass transfer from a gas to a liquid also affects many other industries and chemical processes. In addition to algae utilizing carbon dioxide, bacteria, yeast, and mammalian cells utilize oxygen for aerobic growth, showing the importance of

gas to liquid transfer in cell cultures. Smaller bubbles, and therefore higher mass transfer, increase the speed and efficiency of chemical reactions and manufacturing in which the gas acts as a catalyst as well. Hydroformylation, alkylation, carboxylation, polymerization, and hydrometallurgy are all processes that benefit from smaller bubbles and increased mass transfer rates from a gas to a liquid (Shah et al., 1982).

In addition to fixation of carbon dioxide from air, algae can grow and produce biofuels from intracellular lipids, providing a renewable source of fuel as an alternative to fossil fuels. Algal biofuels have shown promise because even though they release carbon dioxide when burned, they consume carbon dioxide in development, providing a much higher net energy release per carbon dioxide released.

Algae cultures show benefits over other forms of biofuels due to algae farms having higher energy densities and requiring less land to make biofuels than other terrestrial crops such as corn, canola, and switchgrass (Clarens et al., 2010). In addition, algal farms do not compete for land with food crops, decreasing their opportunity cost (Sheehan et al., 1998). Even though algal farms have many benefits, there are a few downfalls such as they are slow growing organisms (~18 hour doubling time), providing nutrients can be costly, and growing algae uses a significant amount of fresh water. In order to minimize the problem of water usage, farms could utilize nutrient rich biofilms, which can reduce the water necessary. Growing algae in wastewater can also minimize the amount of water necessary as well as decrease the cost of providing additional nutrients.

In addition to creating biofuels, algae naturally produce nutraceuticals and other health supplements in the form of carotenoids. These carotenoids, such as lutein, are

antioxidants that work to prevent aging, inflammation, and sun damage. They also improve ocular health and have been used as dietary supplements for fish farming. Lutein, the main carotenoid product of the microalgae *Chlorella vulgaris*, sells for $570-790 per kilogram with a market nearing $1 billion a year with an annual increase of 2.2% (Prommuak et. Al, 2012; Del Campo & García-González, 2007). Algae cells also synthesize beta-carotene, other dietary supplements, polyunsaturated fatty acids, and phycoerythrin, and can be used in cosmetics, polymers, aquaculture feeds, and to make pharmaceutical proteins such as anticancer drugs (Rosenberg et al., 2008).

This thesis addresses the issues of identifying the optimal carbon dioxide feed rate for the microalgae *Chlorella vulgaris* based on the growth rate and productivity of lipids, protein, and lutein. This thesis also addresses how the intracellular components of interest (lipids, lutein, proteins, etc.) change based on night/day growth conditions, mimicking outdoor, large-scale culture conditions. A microfluidic device to generate micro-scale bubbles was created and utilized to decrease bubble size and increase the mass transfer between a gas and liquid. The more efficient microbubbler system was also tested in algae cultures to show the increased mass transfer in bioreactors on a macroscopic level.

Chapter 2
Materials and Methods

2.1 Strain Selection and Culture Conditions

2.1.1 Strain Selection

For all algal experiments, the strain *Chlorella vulgaris* (UTEX 395) was used. This strain was chosen because it is a commonly utilized strain with fast growth and high lipid content (Hallenbeck, 2012).

2.1.2 Culture Media

Cultures were grown with a liquid volume of 500 mL in a salt media commonly used for algae culture, Bold's Basal Media (BBM) (Bischoff & Bold, 1963). BBM media contains 250 mg/L sodium nitrate, 175 mg/L potassium phosphate monobasic, 75mg/L magnesium sulfate heptahydrate and potassium phosphate dibasic, 50 mg/L EGTA, 31 mg/L potassium hydroxide, 25 mg/L calcium chloride dihyrdate and sodium chloride, 11.42 mg/L boric acid, 8.82 mg/L zinc sulfate heptahydrate, 4.98 mg/L iron sulfate heptahydrate, 1.57 mg/L copper sulfate pentahydrate, 1.44 mg/L manganese chloride tetrahydrate, 0.71 mg/L molybdenum trioxide, 0.49 mg/L cobalt nitrate hexahydrate, and 1 μL sulfuric acid. The media was supplemented with 20 mM Tris to prevent pH drops during high carbon dioxide feed conditions and the final pH was adjusted to 6.8.

2.1.3 Culture Conditions

Gas was fed at a flow rate of 400 mL/min (kept constant with a Cole Parmer flowmeter for air and carbon dioxide) via stainless steel, 19 gauge, 4" long, blunt end luer needles and an agitation rate of 200 rpm. Cultures were grown at room temperature (23° C). The

carbon dioxide trials were grown using 12h/12h night/day cycles with the light cycles having an intensity of 10,000 lux (~300 $\mu E/m^2/s$).

The microbubbler culture experiment was run with continuous lighting of 10,000 lux (~300 $\mu E/m^2/s$) with a flow rate of 400 mL/min for the needle and 0.5 mL/min for the microbubbler. The gas supplied was 5% CO_2 in air.

The pH and carbon dioxide gas probes for monitoring cultures were from Vernier and were recorded every minute during trials by LoggerPro software.

2.2 Cell Growth and Size Analysis

2.2.1 Cell Density

Flow cytometry was used to calculate cell density and to analyze the size distribution and color of the cells. A Millipore Guava Flow Cytometer was used to give accurate cell density measurements. The cultures were diluted with Phosphate Buffered Saline (PBS) to a range of 50-500 cells per μL and then sampled to obtain accurate readings.

Hemocytometer counts were also used to verify the cell density using ruled hemocytometer counting chips from Electron Microscopy Sciences along with a Zeiss Axiovert 100 microscope.

For the majority of trials, optical densities were measured for all growth conditions and correlated to cell density. The optical densities for the cultures were measured at a wavelength of 600 nm on a Promega Glomax multidetection spectrophotometer.

2.2.2 Cell Size

The cell size and color were measured using a FlowCam flow cytometer. The cultures were diluted with PBS and run through the detection system, which also took images of each cell passing through the flow cell. The computer automatically computed the size, color, and cell density.

2.3 Intracellular Component Analysis

After lyophilizing frozen samples, the intracellular components were analyzed using various techniques.

2.3.1 Lipid Analysis

Lipid content was analyzed using dried algae biomass in a Dionex Automated Solvent Extractor (ASE) 150 using a 2:1 methanol:chloroform solvent. The solvent was flown through a cell containing the dried biomass at 120°C and a pressure of 200 psi. Three cycles of extraction occurred and then the solvent was evaporated under nitrogen and the dried lipids were weighed.

2.3.2 Protein Analysis

Proteins were extracted from a 2 OD_{600} pellet of algae resuspended in 1 mL of NaOH and heated for 5 minutes at 100°C. Cells were centrifuged for 10 minutes at 12,000 rpm and the supernatant was kept for protein analysis. Protein analysis was done using a BCA assay, measured at a wavelength of 562 nm.

2.3.3 Pigment Analysis

Total chlorophyll, chlorophyll a, and chlorophyll b were analyzed by dissolving 3 mg of dried algae into one mL of 80% acetone in water. They were vortexed on ice in the dark

for 15 minutes. The sample was then centrifuged at 12,000 rpm for 12 minutes and the supernatant was kept for analysis. The supernatant was analyzed at wavelengths of 647 and 664.5 nm using an Ocean Optics SD2000 fiber optic spectrometer. The correlation between chlorophyll concentration and the absorbance at the two wavelengths is shown in Equations 1, 2, and 3 (Inskeep & Bloom, 1985).

$$Total\ Chlorophyll\ \left[\frac{mg}{L}\right] = 17.95 * A_{647} + 7.90 * A_{664.5} \quad \text{[Equation 1]}$$

$$Chlorophyll\ a\ \left[\frac{mg}{L}\right] = 12.63 * A_{664.5} - 2.52 * A_{647} \quad \text{[Equation 2]}$$

$$Chlorophyll\ b\ \left[\frac{mg}{L}\right] = 20.47 * A_{647} - 4.73 * A_{664.5} \quad \text{[Equation 3]}$$

To analyze total pigments, approximately 40 mg of dried algae was dissolved in 5 mL of 3:1 methanol:dichloromethane in the dark and grinded in a mortar by a pestle. This mixture was centrifuged at 10,000 rpm for 10 min at 4°C. The supernatant was collected and the process was repeated with the pellet two more times for a total of 15 mL. The supernatant was then dried under nitrogen and the remaining dried pigments were weighed.

Afterwards, the dried pigments were resuspended in 5 mL of 3:1 methanol:dichloromethane and filtered. The filtered sample was run using reverse phase – high pressure liquid chromatography (RP-HPLC) using a Poroshell 120 column with a pore size of 120 Å. The carrier solvent was 5:85:5.5:4.5 (v/v) dichloromethane:methanol:acetonitrile:water and the elution solvent was 22:28:45.5:4.5 (v/v) dichloromethane:methanol:acetonitrile:water. A diode array detector (DAD)

measuring at a wavelength of 450 nm was used for analysis and lutein eluted at approximately 4 minutes (Figure 1).

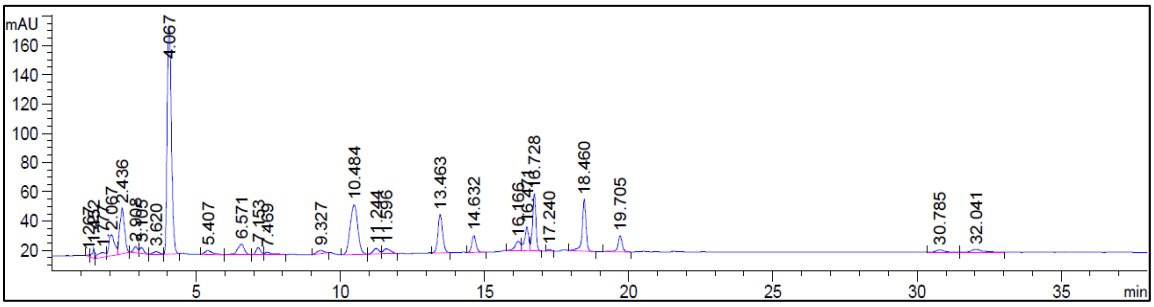

Figure 1. HPLC DAD graph for pigment analysis. The diode array detector (DAD) analyzed the separated HPLC sample at 450 nm. The peak at 4.067 minutes corresponds to lutein.

2.4 Microfluidic Bubbler Construction and Operation

2.4.1 Fabrication

For the fabrication of the microfluidic flow-focusing devices (Figure 2), we used well-developed soft lithography techniques. Negative photoresist (SU-8 3050, Microchem Corp.) was spin-coated onto a silicon wafer (Silicon Inc.) and exposed to a UV light source (KLOÉ) through a negative mask printed on a transparency (Figure 3). The result, after developing, was a silicon wafer with raised structures 60 µm high that act as the master mold. A 10:1 ratio of the elastomer and curing agent, PDMS, is poured over the wafer, cured, and peeled off. Biopsy punches (Ted Pella, Inc.) are used to create inlet ports for the fluid flow. The surface of both the PDMS and a cleaned microscope slide are treated with oxygen plasma and placed in contact to form a bond; the bonded devices are baked at 85° C overnight to enhance this bond.

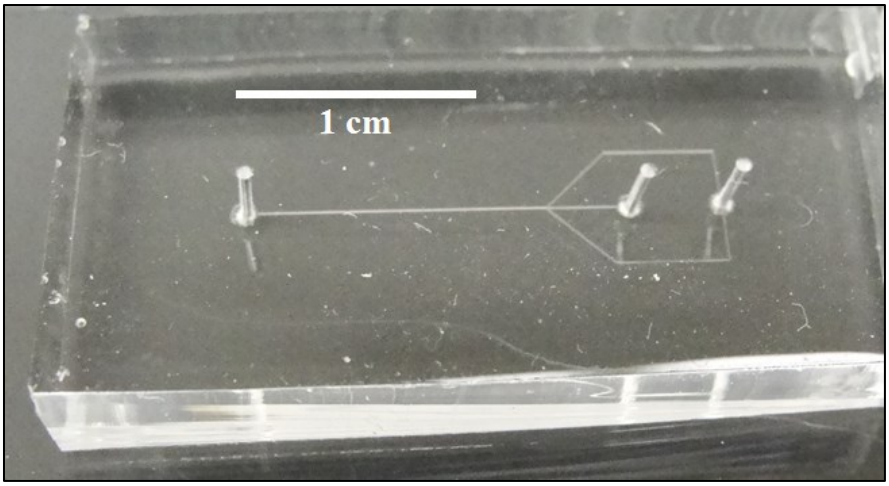

Figure 2. Macroscopic view of microfluidic bubbler. The microfluidic bubbler device, made from PDMS, was attached to a microscope slide and shows the channels in the center of the device.

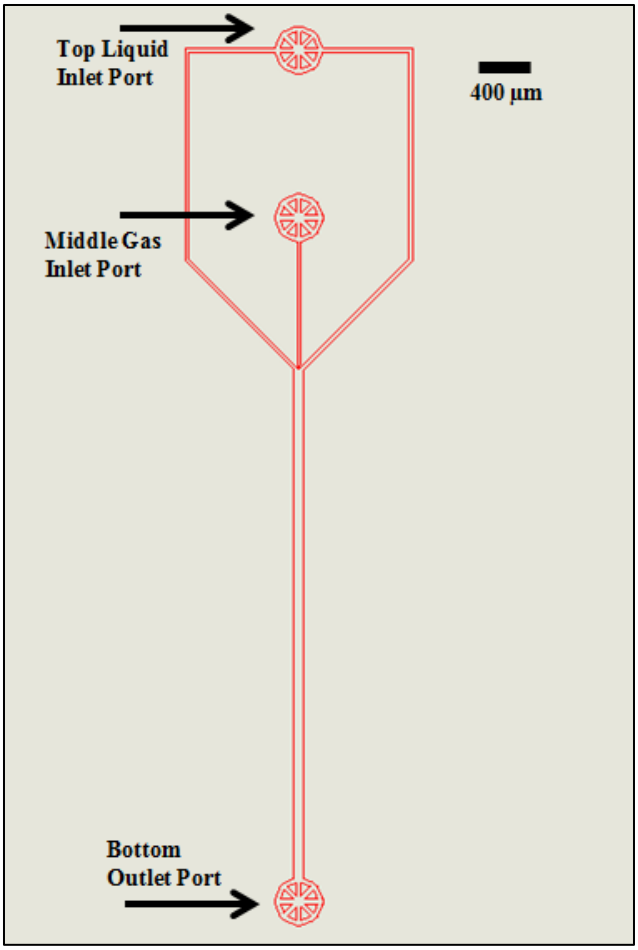

Figure 3. Microfluidic bubbler channel and mask design. Liquid enters through the PDMS to the top port where it splits into two channels. The two liquid channels converge with the gas channel that enters at a central port. These channels combine to form bubbles that exit through the outlet port at the bottom.

Two inlet ports were created at the top and middle of the device. The top inlet port, for liquid, splits into two channels. These two channels converge with a third channel containing the gas, from the middle inlet port, at a 40° angle. These three channels are 25 μm and the gas channel tapers to 10 μm at the junction. The outlet channel is 66.67 μm and leaves from the bottom outlet port. All channels had a height of 60 μm.

2.4.2 Operation

The liquid used for all tests was BBM supplemented with 0.5% pluronic F-68, which served as a surfactant to stabilize bubble formation. The addition of pluronic F-68 showed no negative effects on algal cell growth and has been used in many other cell cultures, including insect and mammalian cultures (Murhammer & Coochee, 1988; Zhang et al., 1992). Air was used as the gas for all K_La testing and air with 5% CO_2 was used in the culture operation of the microbubbler.

Fluid and gas streams are delivered via pressurized cryogenic vials set at nearly identical pressures to deliver microbubbles at a constant flow rate. The bubbles in the microfluidic channels were analyzed with a Nikon TI-E confocal microscope to ensure stable bubbles were formed. To take pictures and videos of the bubbles in the liquid, a Sony Cybershot DSC-H20 camera was used and imageJ was used to analyze the bubble sizes in the liquid.

2.4.3 Comparative Bubbling Equipment

Four common additional methods of supplying gas to liquids for mass transfer were tested against the microfluidic bubbler: an open-tube, needle tips, a common aquatic stone sparger, and an industrial sparger used for bioreactors. The open-tube was a Bellco Glass straight sample metal pipe for a 10 mm port with an inner diameter of 0.5 cm and

an outer diameter of 0.625 cm. The needles used to supply the gas were stainless steel, 19 gauge, 4" long, blunt end luer needles. The common aquatic sparger was the small air stone cylinder from Active Aqua with a diameter of 1.7 inches and a height of 2.0 inches. The industrial sparger was a Bioengineering aeration tube with sinter-metal microsparger for 5L vessel.

2.5 K_La Determination

Values for K_La are difficult to calculate and are usually determined experimentally. To determine the K_La values for different systems, 500 mL of BBM media at 25°C was placed in a beaker with a diameter of 10 cm, giving a liquid height of 6.36 cm. A dissolved oxygen (DO) probe (Vernier) was inserted into the liquid and the liquid was stirred with a magnetic stirrer at a constant agitation rate of 175 rpm. The computer captured and recorded DO readings every second. Initially, air was fed to the bottom of the liquid until the DO stayed constant at the saturation point. Then, nitrogen gas was fed into the culture to drop the DO. Once the DO dropped below 3 mg/L, the gas feed was switched back to air and the DO was monitored (Figure 4).

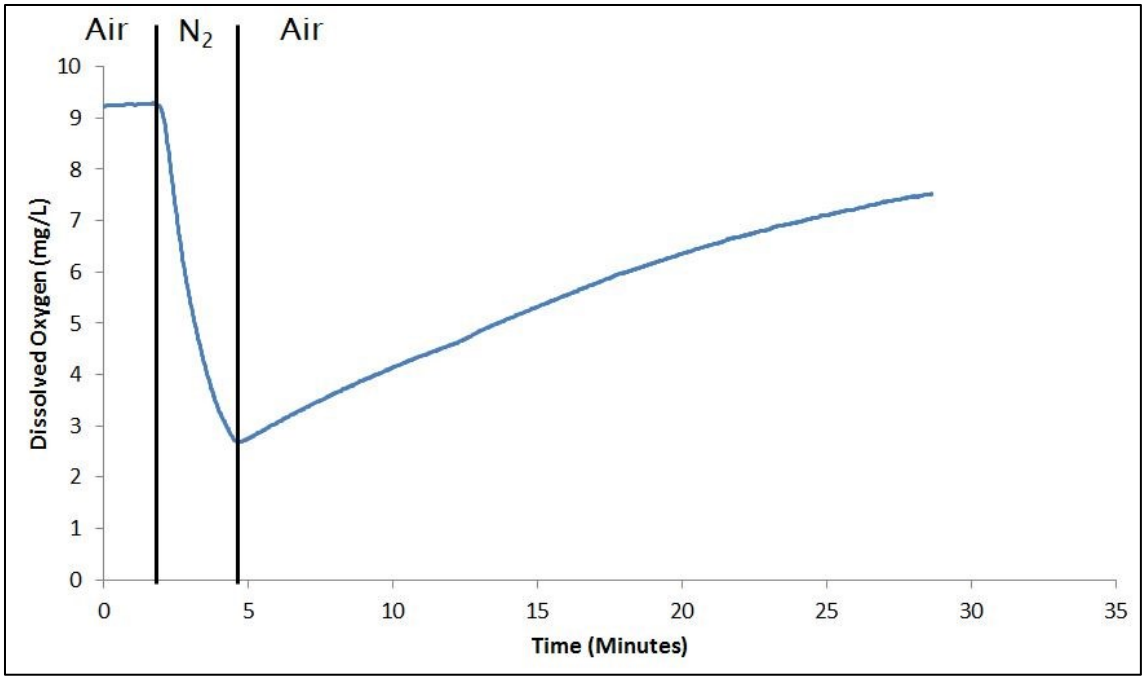

Figure 4. Dissolved oxygen concentration over time for the calculation of K_La. Air was sparged into the system to obtain the baseline dissolved oxygen concentration, then nitrogen gas was sparged into the liquid to remove the dissolved oxygen. After the dissolved oxygen dropped, air was fed back into the liquid and the increase in dissolved oxygen was recorded.

To calculate the K_La, the $\ln(C_a^*-C_a)$ was plotted for the segment of interest after the switch back to air. In this case, C_a^* was the highest concentration of the DO (saturation), achieved at the beginning of the trial, and C_a is the DO for the rest of the trial. For the segment of interest, the resulting graph of the $\ln(C_a^*-C_a)$ over time produced a straight line with a negative slope (Figure 5). The K_La is the slope multiplied by negative one and has units of inverse minutes.

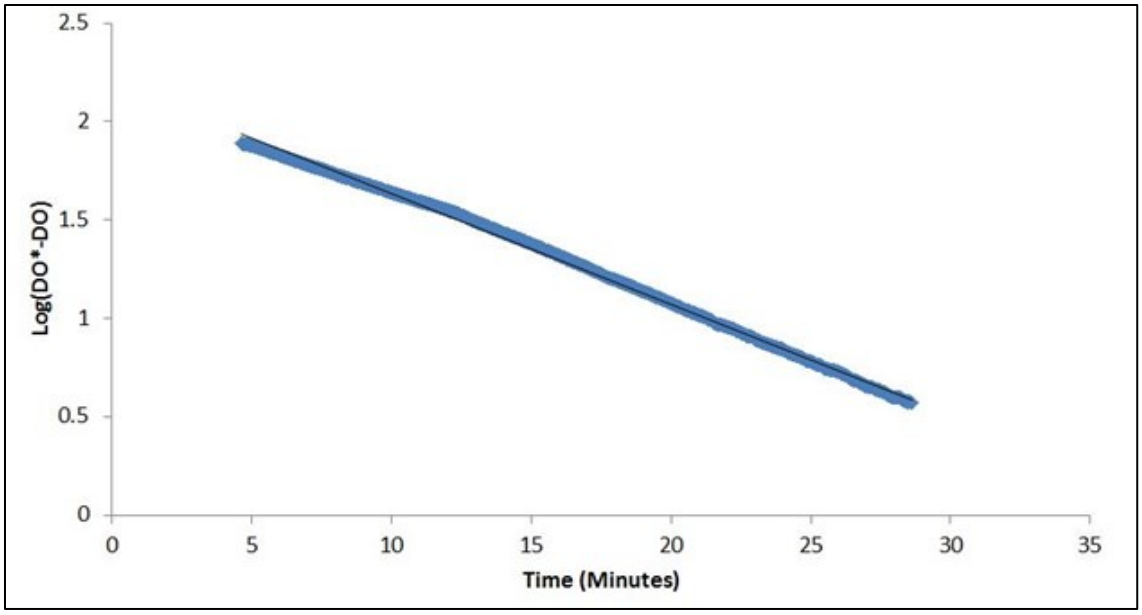

Figure 5. Plot of the natural log of the saturation dissolved oxygen concentration minus the dissolved oxygen levels for the area of interest. The area of interest is the section when air is sparged back into the system after nitrogen gas. The K_La is calculated as the negative slope of the line.

The fraction of oxygen transferred calculations were verified utilizing an oxygen gas sensor with the K_La testing. The oxygen gas sensor was sealed in the off-gas of the liquid of the K_La tests and recorded the oxygen gas concentration every second. An outlet tube for the gas outlet of the system was placed into water to allow gas to flow out of the system without gas flowing from the room air into the system. As nitrogen gas was fed to the liquid, the DO and the oxygen gas concentration decreased. When air was bubbled into the system to test the K_La, the oxygen gas sensor recorded the change in oxygen concentration, which allowed for the calculation of oxygen gas concentration in the bubbles.

The probes to measure dissolved oxygen and oxygen gas for K_La testing were from Vernier and were recorded every second during trials by LoggerPro software.

Chapter 3
Identifying Optimal CO_2 Feed

3.1 Introduction

Algae cells grow and proliferate by absorbing carbon dioxide through photosynthesis to create sugars for cell use. There are two different types of reactions that occur in photosynthesis – light-dependent and light-independent reactions. For the light-dependent reactions, chlorophyll (a pigment) in the thylakoid of the chloroplast absorbs one photon of light, releasing one electron to the electron transport chain, thus creating a H^+ ion differential. This differential between the thylakoid and the stroma, or liquid in the chloroplast similar to the cytosol of a cell, leads to the activity of ATP synthase and $NADP^+$ reductase. The enzymes generate ATP and NADPH in the stroma, which support the light-independent reactions of photosynthesis.

Algal cells have two types of chlorophyll that absorb the light necessary for the light-dependent reactions: chlorophyll a and b. The difference between these two types of chlorophyll is the wavelength of light they absorb and utilize for photosynthesis. Chlorophyll a mainly absorbs violet, blue, and red colors at the ends of the visible spectrum, reflecting green light. Chlorophyll b absorbs light more to the middle of the visible spectrum, blue and orange light, while still reflecting green light.

Once the chlorophyll absorb light and create ATP and NADPH, ribulose-1,5-biphosphate carboxylase/oxygenase (RuBisCO) takes three molecules of carbon dioxide, 6 molecules of NADPH, 5 molecules of water, and 9 molecules of ATP and converts them to one molecule of the three carbon glyceraldehyde-3-phosphate (G3P), 6 $NADP^+$, 9 ADP, 2 H^+,

and 8 inorganic phosphates (P_i). This process occurs in the chloroplast stroma and is light independent.

Photosynthesis, therefore, depends on the amount of light and carbon dioxide the microalgae cells absorb since they are the two substrates that can be limited since the light dependent reactions create the energy needed for RuBisCO in the light-independent reactions. When exposed to sunlight or artificial lighting in labs, cells should be saturated with light, making carbon dioxide the limiting substrate. Many past papers have shown that algae cells have higher photosynthetic rates and faster growth with gases that have a higher percentage of carbon dioxide than ambient air (0.04%), showing carbon dioxide is the limiting substrate with enough light (Yun et al., 1996; Chinnasamy et al., 2009).

Since algae cells grow better with higher levels of carbon dioxide, one sustainable practice has been to grow algae cultures using the flue gas from companies and industrial factories that have high fractions of carbon dioxide in their off-gases. The average flue gas composition is anywhere from 3 to 15% carbon dioxide depending on the type of system, with most systems operating around 12% (Packer, 2009). Knowing what levels of carbon dioxide provide the highest growth rates and CO_2 fixation for algae allows for optimal usage of these flue gases in algal farms.

To compare algae growth rates under varying levels of carbon dioxide, the growth rate must be calculated using cell density. To calculate growth rate, plotting the natural log of the cell density against time yields a straight line. The slope of this line corresponds to the growth rate with units of inverse time.

Another common metric of growth is the dry cell weight, or biomass, and the biomass productivity. The dry cell weight comes from the mass of a set volume of algae after it is dried and the biomass productivity comes from dividing this dry cell weight by the time of the culture (Equation 4).

$$Biomass\ productivity\ \left[\frac{\frac{mass}{volume}}{time}\right] = \frac{dry\ cell\ weight\ [\frac{mass}{volume}]}{time} \quad \text{[Equation 4]}$$

The final calculated parameter discussed is the weight of individual cells after being dried. This value comes from the dried biomass divided by the cell density at the time the dry cell weight was measured, yielding a mass per cell (Equation 5).

$$Cell\ weight\ dried\ \left[\frac{mass}{cell}\right] = \frac{dry\ cell\ weight\ [\frac{mass}{volume}]}{cell\ density\ [\frac{cell}{volume}]} \quad \text{[Equation 5]}$$

3.2 Correlation Between Cell Density and Optical Density

The two main methods for calculating cell density are flow cytometry and counting using a hemocytometer. Flow cytometry counts the cell density by flowing a diluted sample through a thin tube with a laser passing through the tube at a cross-section. Based on the optical properties of cells (the green color in the case of algae), cells will absorb some of the light from the laser, decreasing the intensity of the light passing through the tube. Every time a disruption in the intensity occurs, the computer registers it as an "event". Based on the number of events that occur within the size range of algal cells (4-10 μm for *Chlorella vulgaris*) and the volume used by the system, the computer calculates the number of cells per volume (Ting et al., 1991).

The other way to measure cell density, via hemocytometer, utilizes a microscope and specialized microscope slides. A diluted sample of the culture is placed on a gridded slide

and the number of cells within each grid is counted. Based on the average number of cells in all of the grids, the known dilution factor, and the known volume of each grid, the cell density can be calculated.

However, many problems arise in the sampling of both measurements in terms of the method of measuring, repeatability due to clumping of cells, and manual errors in dilutions. Therefore, a common way to measure the growth and health of a culture is using optical density, which measures how much light is absorbed by the sample at a specific wavelength. Optical density provides a fast, efficient, and reproducible way to measure algal cultures. A common wavelength used to measure algal cultures is 600 nm (Estevez, 2001).

To be able to know the cell density based on optical density, a standard curve was created using the optical density at 600 nm, flow cytometry using a Guava flow cytometer, and a hemocytometer (Figure 6).

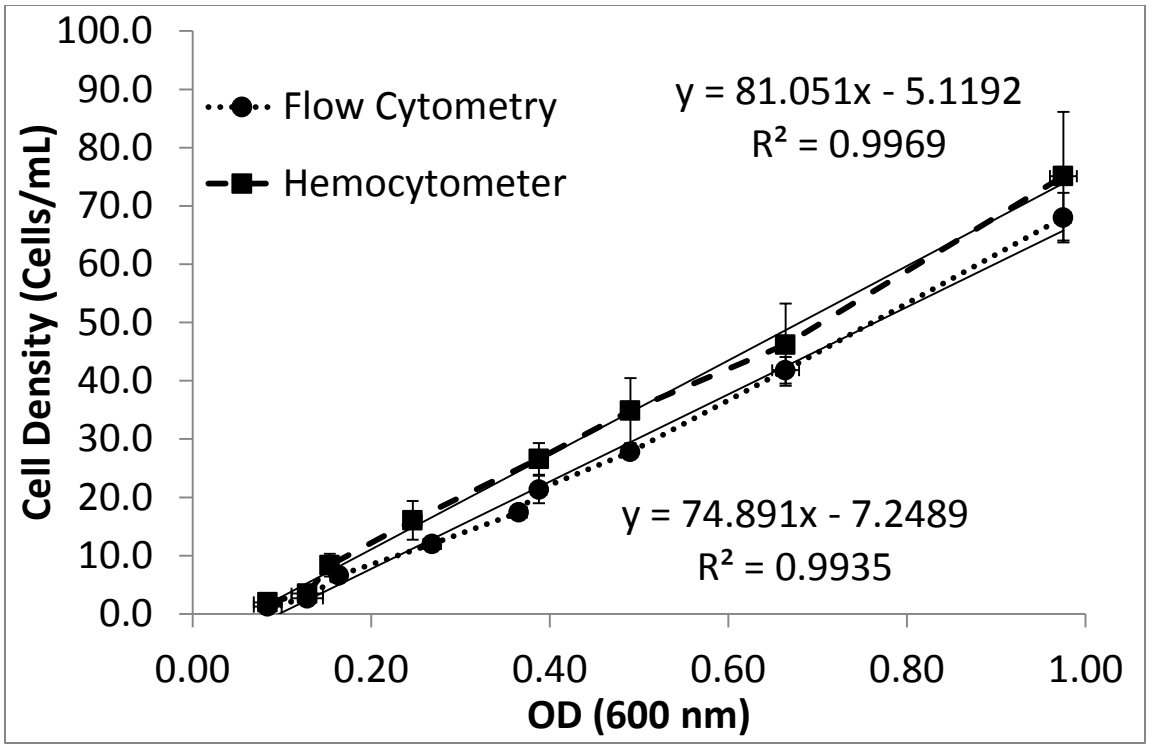

Figure 6. Cell density dependence on optical density. The cell density was measured with a flow cytometer and hemocytometer at varying optical densities to determine a correlation. Both measurements showed strong correlations. The two correlations were averaged to a correlation of cell density = 78.0* OD_{600} – 6.2.

As shown in Figure 6, the cell density, measured by flow cytometry and a hemocytometer, both show linear correlation with optical density at 600 nm. Due to the error of the sampling and measurements known to occur with cell density, an average trend line was calculated for use in calculating cell density from optical density from both methods, shown in Equation 6.

$$Cell\ density = 78.0 * OD_{600} - 6.2 \qquad \text{[Equation 6]}$$

3.3 Growth Under Varying CO_2 Conditions

The cell density, calculated from optical density, helps to calculate the growth rates for the algae cultures tested under varying carbon dioxide feed rates to identify the optimal carbon dioxide concentration for fastest growth. The growth of *Chlorella vulgaris* was

tested under 0.04 (room air), 3, 5, 10, and 12.5% carbon dioxide to compare their growth and high value component production. Figure 7 shows the growth under these varying carbon dioxide concentrations, measured by optical density, using night and day cycles. All cultures underwent an approximately 100-hour lag phase followed by the standard exponential and stationary phases of algae growth (Yan & Pan, 2002).

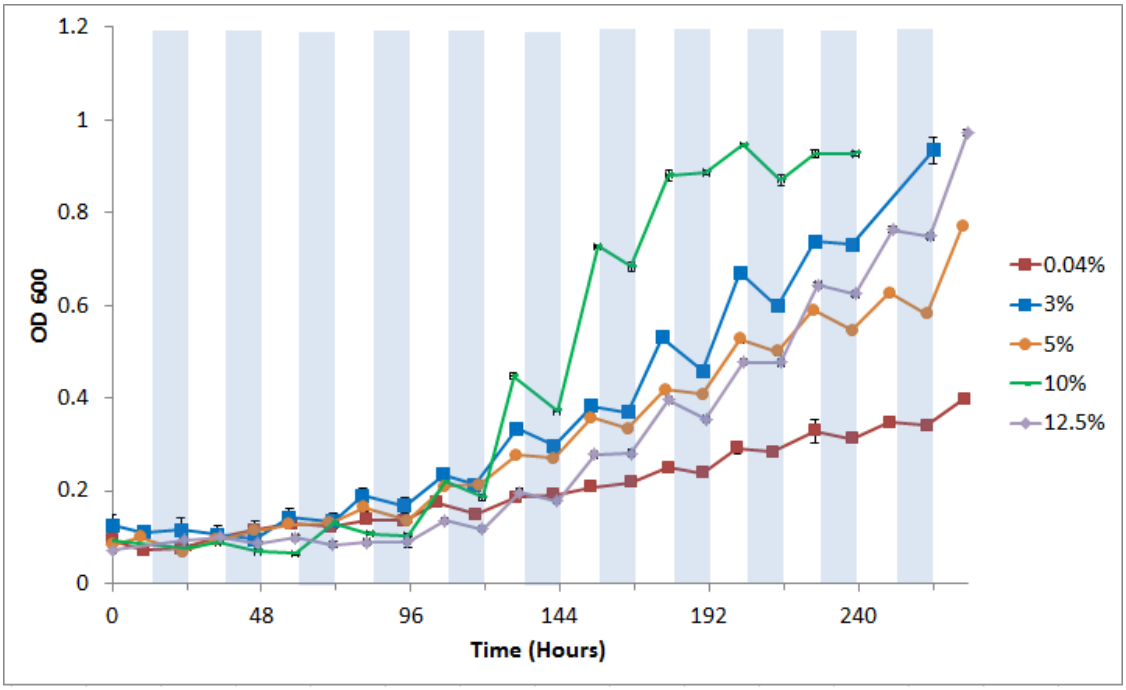

Figure 7. Growth curve for *Chlorella vulgaris* under varying carbon dioxide feeds. All cultures underwent an approximately 100-hour lag phase followed by an exponential phase. The 10% culture grew the fastest and all cultures only grew during light cycles and dropped slightly in optical density during the dark cycles (shaded bars).

To compare the numerical differences of the growth, the total growth rates were calculated for all the cultures as well as the growth rate for only the light cycles, since the cells do not grow during the dark (Table 1). The drops in optical density during the dark periods are investigated and explained in section 3.5. The 10% carbon dioxide feed had the largest growth rate, followed by 12.5, 3, 5, and then 0.04%. In addition, the growth rates for only the light cycles were all approximately double the total growth rate, which

follows the trend of the cells spending exactly half of their time in the light and the other half in the dark.

Table 1. Growth rates for *Chlorella vulgaris* under varying carbon dioxide feeds. The growth rates show that the 10% trial grew fastest followed by 12.5, 3, 5, and 0%. The growth rates for only the light cycles were approximately double that of the total growth rate, corresponding to a 12/12 light/dark cycle.

Carbon Dioxide Feed Percentage	Total growth rate (1/hr)	Light growth rate (1/hr)
0.04%	0.010 ± 0.001	0.019 ± 0.002
3%	0.017 ± 0.003	0.033 ± 0.004
5%	0.014 ± 0.002	0.029 ± 0.004
10%	0.032 ± 0.008	0.064 ± 0.017
12.5%	0.018 ± 0.002	0.036 ± 0.005

There was an increase in growth rate with higher carbon dioxide feeds up to 10%. The 12.5% culture had a lower growth rate due to a more significant drop in pH due to the higher carbon dioxide feed (Table 2). This pH drop caused the 12.5% culture to have a longer lag phase to allow the cells to acclimate and naturally adjust the pH because algae cultures prefer slightly basic conditions and typically increase the pH of a culture. Table 2 also shows that the room air (0.04% CO_2) culture increased in pH as did all of the other cultures once the media pH was changed due to the carbon dioxide feed. Once the pH of the 12.5% culture returned to normal, the cells grew fast, leading to the second highest growth rate.

Even though these systems were buffered with tris, which is known to absorb and desorb CO_2, it seems that the 12.5% provided more CO_2 than the tris could absorb and buffer in the system. More CO_2 than the tris could buffer could have led to the larger drop in pH,

leading to a longer lag phase for the cells to acclimate and adjust the pH back into the optimal range.

Table 2. Initial and final culture pHs under varying carbon dioxide conditions. All cultures started at similar pHs and, except for the room air (0.04%), dropped in pH immediately after the addition of higher carbon dioxide concentrations. After the initial drop in pH, all cultures rose in pH.

Carbon Dioxide Feed	Initial pH	pH 1 Minute After Gas Feed Began	Final pH
0.04%	6.8	6.8	7.2
3%	6.8	6.5	7.5
5%	6.8	6.4	7.3
10%	6.8	6.3	6.6
12.5%	6.8	5.3	6.5

3.4 Cellular Component Differences in Different CO_2 Conditions

Based on the application, specific intracellular components of microalgae have relatively high value. The components of interest (lipids, protein, and lutein) were analyzed at the end of the culture to see what the optimal carbon dioxide feed would be depending on the downstream application of the culture.

Figure 8 shows the comparison between the dry cell weight, biomass productivity, weight of each cell after being dried, protein concentration, and lipid content for each of the different carbon dioxide concentrations at the end of the culture. The dry cell weight and biomass productivity correlated with the growth rates, indicating the faster the growth, the faster the culture accumulated biomass.

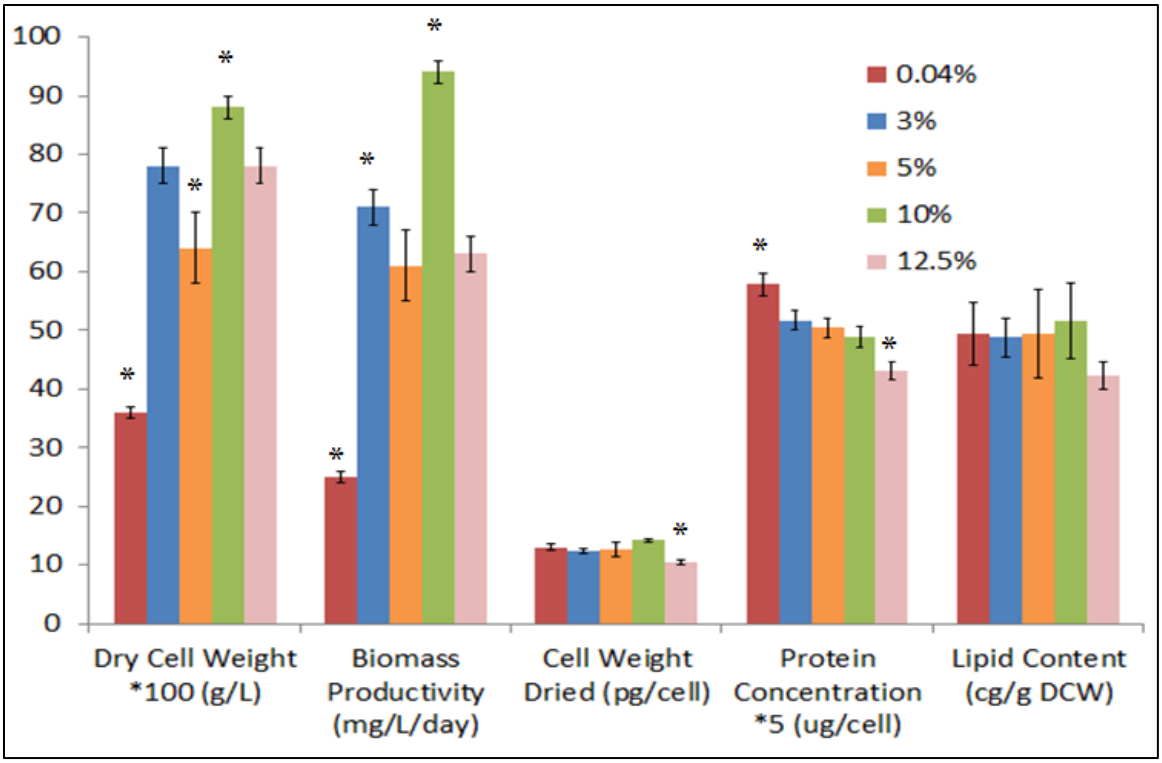

Figure 8. Dry cell weight, biomass productivity, cell weight, protein concentration, and lipid content for varying carbon dioxide concentrations. The dry cell weight and biomass productivity correlated with growth rate. Cell weight of individual cells and lipid content stayed approximately constant among carbon dioxide concentrations. The total protein concentration decreased with increasing flow rate of carbon dioxide. * indicates statistical significance with 95% certainty.

The weight of each cell after lyophilizing stayed approximately equal for each concentration, indicating the extra carbon dioxide did not accumulate within the cell, but rather only increased growth. It has been shown that with increasing carbon dioxide concentration, algae cells, specifically *Chlorella vulgaris*, accumulate a higher percentage of carbohydrates within the cell and excrete larger amounts of carbohydrates to rid of excess carbon (Drake & Gonzàlez-Meler, 1997; Gordillo et al., 1999; Chinasamy et al., 2009).

Total protein concentration seemed to decrease with increasing carbon dioxide concentration, similar to the results of others (Drake & Gonzàlez-Meler, 1997; Gordillo

et al., 1999). Due to the lower protein content per cell, it seemed that the proteins left in the cell were more efficient, especially photosynthetic proteins. An alternative explanation would indicate that all proteins kept the same efficiency with some proteins not produced at all. From either explanation, the increased amount of carbon available drove down the protein concentration per cell since other intracellular components, such as carbohydrates, have a relatively larger carbon content and are more readily made and stored for energy. Cells want to utilize the larger concentration of carbon, so they shift from protein production, an inefficient means of storing the carbon, to a more efficient method of storage.

The lipid content seemed to stay approximately constant except for the slight drop with 12.5%. These results coincide with results from others showing slight decreases at high CO_2 concentrations while not having significant differences in lipid content between lower concentrations (Lv et al., 2010).

Additionally, the concentrations of chlorophyll and the carotenoid, lutein, which is used as a health supplement, were determined at the end of the culture (Figure 9). The concentration of total chlorophyll, chlorophyll a, and chlorophyll b all stayed approximately equal for every carbon dioxide concentration. Because there were higher growth rates for the higher carbon dioxide concentrations, there were higher rates of photosynthesis. The higher rates for photosynthesis coupled with equal amounts of chlorophyll indicate more efficient chlorophyll, rather than a larger number, to cope with higher carbon dioxide consumption.

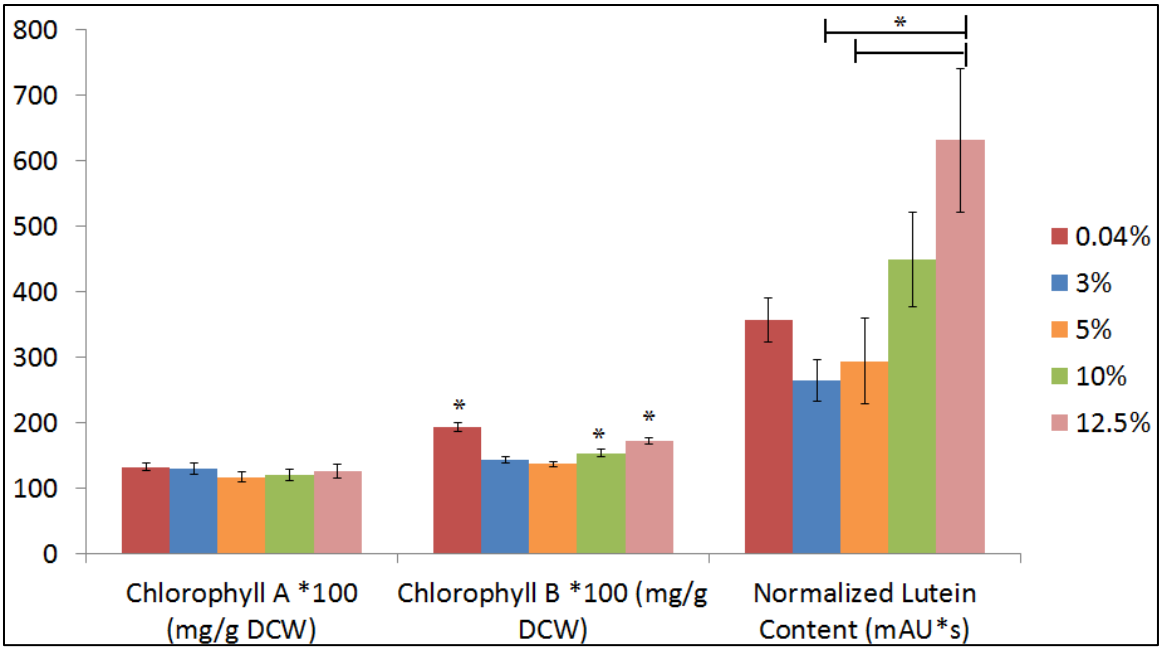

Figure 9. Chlorophyll and lutein content for all carbon dioxide feeds. Chlorophyll concentration stayed approximately constant among all carbon dioxide concentrations. Lutein content increased with increasing carbon dioxide feed. * indicates statistical significance with 95% certainty.

The relative lutein content increased with carbon dioxide concentrations, possibly to deal with the added stress of higher carbon dioxide in the media. Shown in Figure 10, CO_2 gas dissolves into aqueous CO_2 and reaches a steady state with bicarbonate (HCO_3^-), carbonate (CO_3^{2-}), and carbonic acid (H_2CO_3) (Widjaja et al., 2009). Higher CO_2 gas concentrations lead to higher concentrations of all other components (bicarbonate, carbonate, and carbonic acid) based on steady state kinetics. Carbonate and bicarbonate are free radicals due to unpaired electrons, which can cause oxidative damage to cells (Veselá & Wilhelm, 2002). Since lutein is a carotenoid, and therefore classified as an antioxidant, the increased lutein concentration could have helped prevent oxidative damage from the increased concentration of free radicals caused by higher CO_2 levels. The increased lutein concentration could also be the component to counteract the drop in protein production since the cells have equal masses throughout the trials.

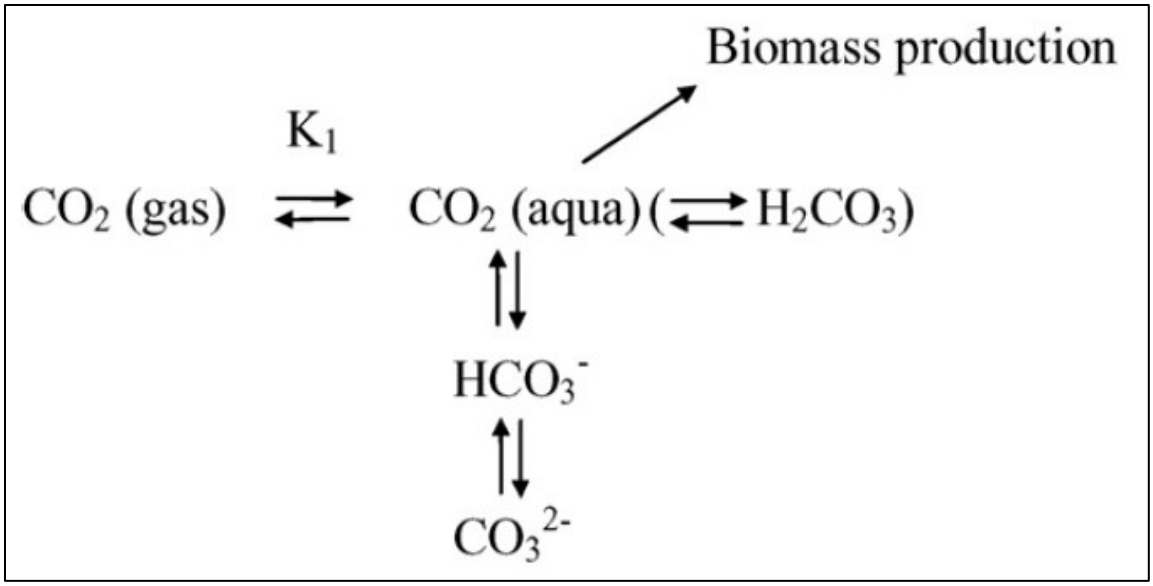

Figure 10. Carbon dioxide reactions in aqueous media. Carbon dioxide converts from gas to liquid CO_2 which than reacts and reaches a steady state with carbonic acid (H_2CO_3) and bicarbonate (HCO_3^-) in the liquid. Bicarbonate also reacts aqueously and reaches a steady state with carbonate (CO_3^{2-}). Figure from Widjaja et al., 2009.

3.5 Light Versus Dark Cycle Variations

Even though the cells do not grow during the dark cycles, significant changes did occur within the cells. Figure 11 shows the dry cell weight, weight of individual dried cells, protein concentration, and the lipid content at the end of a light period compared to the end of a dark cycle. The dry cell weight decreased 31% from 0.64 g/L in the light to 0.44 g/L in the dark. This drop in total dry cell weight stemmed from the 33% drop from 13 pg/cell in the light to 8.7 pg/cell in the dark for the individual weight of each cell.

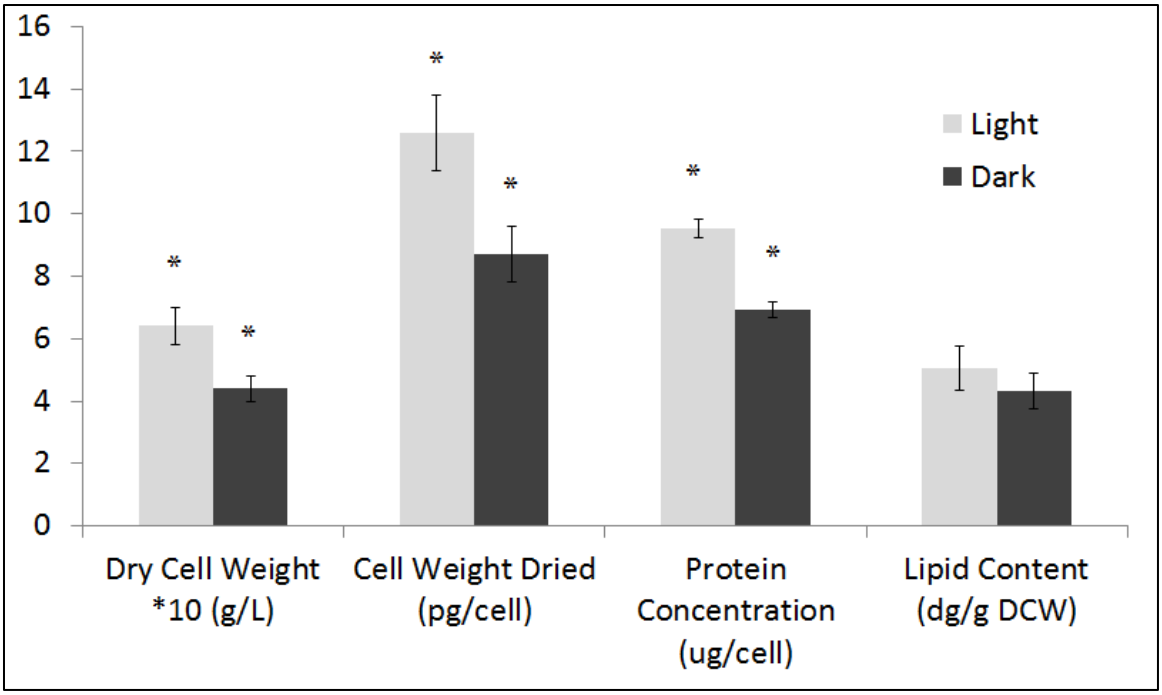

Figure 11. Dry cell weight, individual cell weight, protein concentration, and lipid content for night and day cycles. The dry cell weight decreased during the dark cycle, stemming from decreases in individual cell weights. The decreased individual cell weight was due to drops in intracellular components, such as total protein and lipid, which were consumed to provide energy for the cells during the dark. * indicates statistical significance with 95% certainty.

After seeing the drop in weight of each individual cell, the concentrations of the components of interest (lipids, total protein, and pigments) were investigated. The total protein concentration dropped 27% from 9.5 µg/cell in the light to 6.9 µg/cell in the dark. The lipid content also dropped 14% from 500 to 430 mg/g dry cell weight.

These drops help to explain the decreased individual cell weight and total dry cell weight, which could arise from diminishing concentrations of other intracellular components as well. In the light, cells require energy for growth, reproduction, metabolite production, and maintenance. However, during the dark, when photosynthesis and primary metabolism are inhibited, cells still require energy for maintenance for survival (Chen & Johns, 1996). This required energy likely came from the consumption of intracellular

components, such as carbohydrates, since the degradation of these components releases energy when they cannot create energy from photosynthesis.

After seeing the drop in cell weight, the size of the cells was investigated as well. The FlowCam recorded the equivalent spherical diameter (ESD). The ESD estimates the cells as perfect spheres to calculate diameter since cells are rarely perfect spheres. These measurements were recorded at the end of the light and dark cycles, ignoring anything below 1.5 µm as probable debris from the media or cells. The light cycle cells averaged a diameter of 3.35 µm (Figure 12A) while the dark cycles averaged a diameter of 3.25 µm (Figure 12B). The diameters fell close to each other and show that the cells did not shrink in size during the dark cycles. This led to the assumption that the drop in individual cell weight came solely from a loss of intracellular components and not a decrease in cell size or membrane components. The light cycles had a wider distribution of cells, most likely because cells were dividing during the light cycle, giving rise to larger and smaller cells just before they divide and immediately after they divide, respectively.

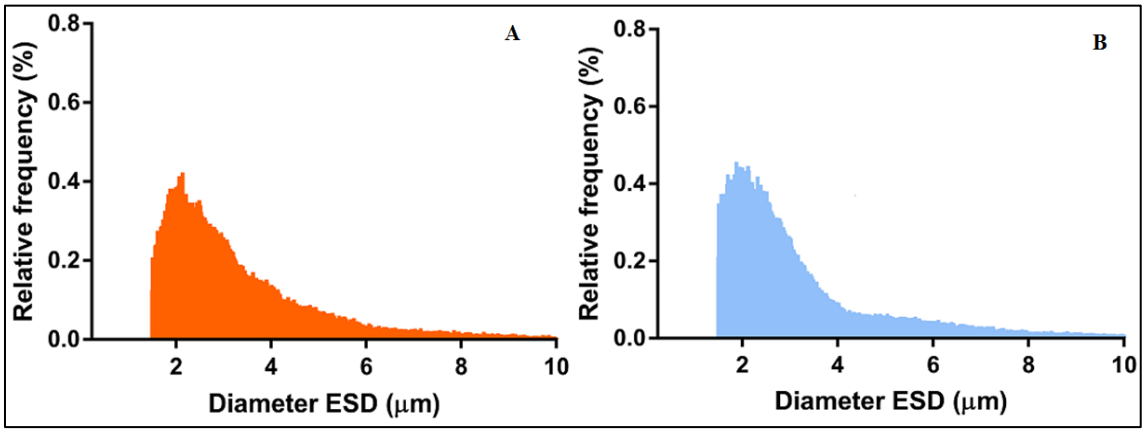

Figure 12. Cell size distribution of light and dark cycles for the 12.5% reactor. The light cycle cells averaged a diameter of 3.35 and the dark cycle averaged 3.25 µm. The light cells had a wider distribution.

The chlorophyll and lutein concentrations between the night and day cycles were also analyzed (Figure 13). The chlorophyll concentration (total, a, and b) all stayed approximately constant, indicating a drop in activity during the night cycle did not affect concentration. Previous studies have shown that cultures in constant darkness have significantly lower levels (~90%) of chlorophyll than in illuminated cultures; however, there was no drop between light and dark chlorophyll concentrations for these trials, suggesting 12 hour night/day cycles were not long enough to cause a decrease in chlorophyll content (El-Sheekh et al., 2012). The green color parameter measured by the FlowCam found that the light and dark cycles had approximately the same amount of green color, verifying similar amounts of chlorophyll.

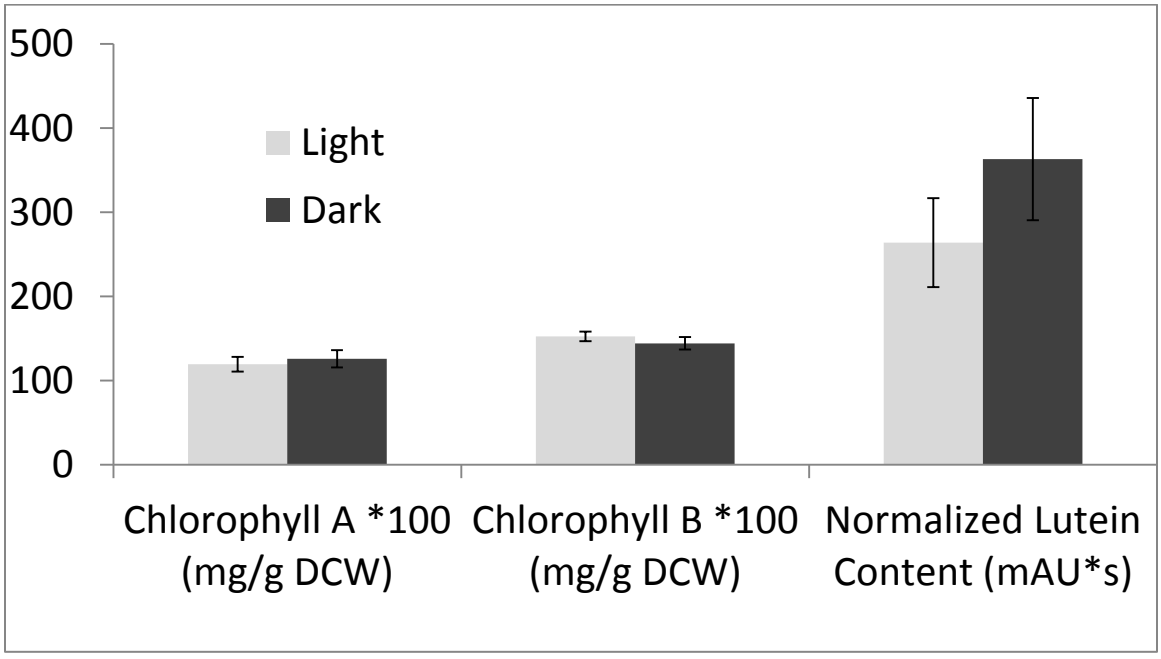

Figure 13. Chlorophyll and lutein concentration in night and day cycles. Chlorophyll levels stayed approximately equivalent while lutein concentration increased during the dark cycles.

The relative lutein content increased 38% during the dark cycle as compared to light cycles. Lutein concentration may have increased to utilize its antioxidant properties to

prevent more free radical damage during the dark. There would have been more free radical damage in the dark than light because there would have been a higher carbon dioxide concentration in the media without the cells consuming the carbon dioxide since metabolism is disrupted in the dark without photosynthesis. The increase in lutein to protect against free radicals in the dark stays consistent with the results from increasing carbon dioxide feed, as previously discussed in section 3.4.

The drops in OD most likely came from the loss of intracellular components and cell weight. These drops would make the cells less dense, absorbing less light and dropping the OD measurements at the end of the dark cycles.

3.6 Economic Analysis

An economic analysis was performed for each of the components of interest to find the optimal carbon dioxide feed depending on the downstream application of the culture (Table 3). The analysis included the cost of adding additional carbon dioxide, a more expensive gas than air, to the culture. These costs could be decreased and possibly eliminated if the algae cultures were set next to power plants to utilize cheap flue gases. The economic analysis yielded that the 10% carbon dioxide feed would be the most efficient, in terms of time and money, to produce all of the desired components.

Table 3. Economic analysis of carbon dioxide feed concentrations. The 10% CO_2 feed provided the highest biomass, protein, lutein, and lipid productivity per volume, time, and dollar spent on feed gases.

Carbon Dioxide Feed	Biomass Productivity (mg/L/day/$)	Protein Productivity (ug/L/h/$)	Lutein Productivity (Lutein/L/h/$)	Lipid Productivity (mg/L/h/$)
0.04%	0.64	25.3	0.65	0.32
3%	2.16	79.1	3.74	1.06
5%	1.72	56.3	2.70	0.84
10%	3.04	87.6	9.04	1.58
12.5%	1.64	59.5	7.77	0.69

3.7 Carbon Dioxide Feed Conclusions

From the gathered results, specific culture conditions can be recommended based on the desired product of the culture. The growth rate of the cells affects the total amount of product as does the intracellular concentration of the product under the different conditions; therefore, both the growth and intracellular concentration will determine optimal conditions. These recommendations include specific carbon dioxide concentrations and whether the cultures will best produce what is desired in the light or dark.

The dry cell weight and biomass productivity correlated with the growth rates, indicating faster growth yields faster biomass accumulation. Therefore, for biomass and dry cell weight, 10% carbon dioxide with continuous lighting provides the ideal culture condition, even with the increased cost of the gas.

Protein concentration decreased slightly with increasing carbon dioxide concentration. Even though the 10% culture costs more than ambient air, which had the highest protein concentration, the 10% culture reached a higher cell density, and therefore total protein

content, much faster. Due to the faster growth, 10% carbon dioxide in continuous lighting should be the ideal condition for protein production.

The lipid concentration stayed relatively constant among all carbon dioxide concentrations, making lipid production solely a decision of growth rate and cost. Similar results were found for chlorophyll concentrations. Thus, due to the fast growth rate and high cell density, lipid and chlorophyll production should be performed at 10% CO_2 in continuous lighting, which outperforms the cost increase.

Lutein concentration increased with increasing carbon dioxide concentration, making 12.5% the ideal concentration for total production in terms of intracellular concentration. However, the 10% trial reached a higher cell density faster because there was not a large pH drop. Because of the faster growth rate and increased cost of the 12.5% condition, the 10% carbon dioxide feed yielded the highest lutein production per time per dollar. The lutein concentration also increased during the dark cycles. Therefore, 10% carbon dioxide for growth in light followed by a night cycle would be the recommended conditions for lutein production. With a more buffered system or pH control, higher CO_2 percentages could lead to more ideal conditions for lutein production.

With increasing carbon dioxide concentration, there seemed to be a redistribution of intracellular components to accumulate carbohydrates and lutein while decreasing protein concentration and keeping other components, such as lipids, approximately equal. Between night and day cycles, there was likely a redistribution of components to accumulate antioxidants, such as lutein, to prevent damage from free radicals while consuming other components, such as proteins, carbohydrates, and lipids, to produce

energy while photosynthesis and metabolism were inhibited. The optimal feed of 10% came from large pH drops with concentrations above 10% and probably not an oversaturation of carbon dioxide. Algal cells could possibly consume more carbon dioxide if the pH drops were not present in the culture, as evidenced by the eventual growth of the 12.5% culture. Therefore, cultures could possibly grow better in higher CO_2 feeds with a more buffered system (more than 20 mM Tris) or with a constant base addition to keep the pH from dropping. Another method to test higher CO_2 percentages would be to find a way to increase the transfer of carbon dioxide to the culture so less carbon dioxide can be fed to avoid pH drops. An increased transfer would allow for higher carbon dioxide feed testing to identify the true optimal amount of carbon dioxide cells can utilize and would provide significant cost decreases due to lower gas feeds to bioreactors.

Chapter 4
Microfluidic Bubbling Device

4.1 Gas Transfer

As previously mentioned, mass transfer from gases to liquids is a critical step in many processes and reactions, especially in industrial settings. Finding a more efficient transfer of carbon dioxide will also allow the determination of the true optimal amount of carbon dioxide algae cells can consume. In addition to improving algae growth, improved mass transfer also aids CO_2 fixation, especially from flue gases before they are emitted into the atmosphere. Flue gases contribute to approximately 7% of the world's carbon dioxide emissions, so lowering the concentration of carbon dioxide in flue gases would significantly lower this percentage (Kadam, 2002). Using a microfluidic bubbler to increase the mass transfer of carbon dioxide from gas to liquid will help fix more carbon dioxide, thus helping the environment by lowering carbon dioxide emissions from flue gases.

Additionally, mass transfer from a gas to a liquid plays a critical role in many multiphase processes spanning multiple industries. Some example applications of gas to liquid transfer occur in biological processing in cell culture bioreactors and other applications such as gas sequestration, chemical manufacturing (hydroformylation, alkylation, carboxylation, and polymerization) and hydrometallurgy (Shah et al., 1982). In most cases, especially in industrial settings, companies and researchers desire an optimal transfer of the mass to the liquid in order to minimize the amount of gas fed to the multiphase processor.

Obtaining a high mass transfer rate is ideal for processes that occur rapidly, such as microbial fermentation, because the dissolved solute has to be replenished quickly. For other processes such as carbon sequestration or applications involving expensive gases, the goal is to achieve the highest fraction of the gas transferred to the liquid. For example, algal cells absorb carbon dioxide, which can then be converted to lipids for the production of biofuels. In addition, microbes can serve to capture carbon dioxide from the atmosphere as one potential approach to lower the carbon dioxide concentration in the atmosphere and reduce the accumulation of this greenhouse gas. Similarly, oxygen sparging is critical to aerobic respiration for bacteria producing biochemicals and mammalian cell lines generating biopharmaceuticals. However, much of the carbon dioxide or oxygen fed to the bioreactors is not successfully dissolved into the liquid broth and as a result, the undissolved gas can pass directly through the bioreactor unused. In these cases, the energetic output and costs associated with the gas sparging are wasted and must be repeated until sufficient solute is dissolved in the target liquid media.

Alternatively, it would be highly desirable to deliver a higher fraction of the feed gas into the liquid solution as part of these multiphase processes, which can be accomplished by creating small, micro-scale bubbles. Microbubbles also have uses in flocculation for harvesting cells from bioreactors, such as algae (Hanotu et al. 2012).

The process of the mass transfer from gas to a liquid occurs in three steps according to Whitman's two-film theory of gas absorption (Whitman 1962). The first step involves the transfer of the component from the bulk of the gas, through the gas boundary layer, and to the phase boundary between the gas and liquid (Figure 14). Differences in partial

pressures provide the driving force for this first step. The gas phase boundary layer is the thin layer of gas next to the phase boundary.

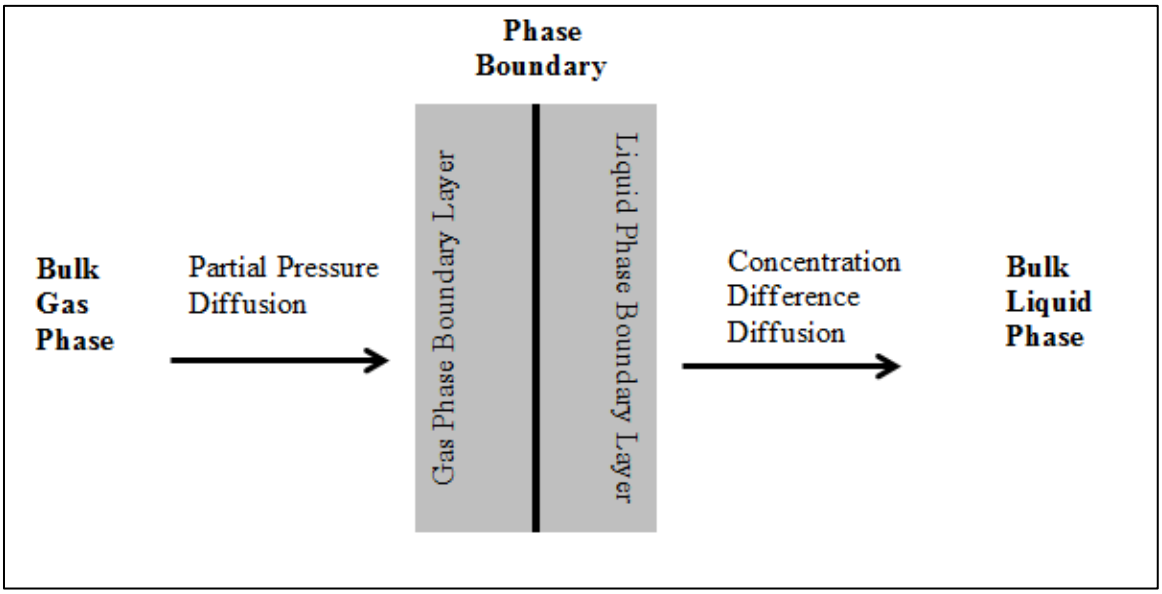

Figure 14. Gas – liquid phase boundary. Mass, such as carbon dioxide, passes from the gas through the gas phase boundary layer, the phase boundary, and finally the liquid phase boundary layer to reach the final state as a dissolved component in the liquid.

The second step involves the instantaneous transfer across the phase boundary between the liquid and gas; this step is assumed to be extremely rapid and in equilibrium relative to the other steps (Figure 14).

The third step transfers the component from the phase boundary through the liquid boundary layer to the bulk liquid. This step depends on the difference in concentration of the component in the liquid for the driving force (Whitman, 1962). From the bulk liquid, the dissolved component can then undergo other steps through chemical reactions or transport into cells. The overall transfer rate (N_a) from the bulk gas to bulk liquid depends on the volumetric mass transfer coefficient (K_La) and the concentration difference or driving force ($C_a^* - C_a$) (Equation 7).

$$N_a = K_L a \cdot (C_a^* - C_a) \qquad \text{[Equation 7]}$$

The overall driving force depends on the resistance of the component to diffuse through the gas boundary layer and the liquid boundary layer. For gases that are poorly soluble in liquids (e.g. oxygen and carbon dioxide in water) the gas will slowly diffuse through the liquid boundary layer to the bulk liquid. The slow diffusion leads to a large liquid phase resistance compared to the gas phase resistance, which diffuses quickly. Since the liquid phase resistance dominates, the overall driving force depends on the difference in concentration in the liquid. Because these tests were performed with oxygen in a salt media mainly composed of water and the results applied to carbon dioxide, the difference in concentration is used as the overall driving force.

Alternatively, for gases that are highly soluble in liquid (e.g. ammonia in water), the gas will dissolve into the liquid and move through the liquid boundary layer much quicker relative to poorly soluble gases. This quick diffusion leads to low resistance from the liquid phase, making the gas phase resistance more dominant. Since the gas phase resistance dominates for highly soluble gases, the overall driving force would be differences in partial pressure.

Therefore, the overall transfer rate depends on three factors: the overall mass transfer coefficient (K_L [distance/time]), the driving force in terms of concentration difference between the solubility limit in the liquid (C_a^*) and the dissolved solute concentration (C_a), and the ratio of surface area to volume for the gas-liquid interface (a [distance^{-1}]). While the driving force (C_a* - C_a) can be increased by decreasing the temperature, increasing

the overall pressure of the system, or by feeding pure gas instead of diluted gas, these approaches may not be feasible and can add to the overall costs.

Another option to increase mass transfer is to increase K_L by increasing the mixing or turbulence, but this will also lead to increased energy input. Alternatively, the interfacial area contribution may have the largest impact on mass transfer and represents a significant opportunity to improve the overall transfer rate. One approach is to take advantage of the fact that surface area to volume ratio, a, depends inversely on the characteristic bubble length. In this way, improved control and reduction in the size or distribution of the size of bubbles can increase mass transfer effectiveness.

By lowering the bubble size, one can also lower the bubble velocity and conversely increase the bubble rise time. In this way, the overall time spent on interfacial gas exchange can be enhanced by decreasing bubbler diameter. Given the importance of bubble size to mass transfer for biological and other processes, methods dedicated to greater control bubble size will become increasingly important in order to enhance chemical and biochemical interfacial process sustainability.

Obtaining the highest possible mass transfer rate is important for faster growth of microalgae as well as the most efficient capture of carbon dioxide in the feed gas. For almost every process, the operators desire maximal transfer of the gas of interest to the system, especially if an expensive gas is used for the process.

4.2 Microfluidic Device Design

Microfluidics is a useful tool for generating and controlling micron-scale gas bubbles and manipulating bubble interfacial area, rise time, and consequently the mass transfer rate and efficiency.

Previous researchers have used microfluidic devices to generate bubbles and drops for a variety of different applications. For example, T-shaped channel junctions have been used to create micro-emulsifications of monodispersed bubbles, anisotropic particles in the microchannels, and to generate and control microbubbles in oil (Garstecki et al., 2005). A variety of different channel geometries have been utilized, including 2-D and 3-D flow focusing devices, T-junctions, and parallel channels (Martinez, 2009; Garstecki et al., 2006). These tests have been performed for a variety of Reynolds numbers in different settings, primarily for bubble creation into liquids with high viscosities in microscopic settings (Garstecki et al, 2005).

Based on previous flow-focusing microfluidic devices to create small bubbles in oil, microchannels for microbubble production were created in polydimethylsiloxane (PDMS) for macroscopic use of transferring mass from a gas to liquid (Garstecki et al., 2005). Fabrication details for these microbubblers can be found in section 2.4.1.

Instead of using the common T-shaped junction in a flow-focusing microfluidic device, a slightly different, Y-shaped junction was utilized to produce micro-scale bubbles in liquid (Figure 15) (Garstecki et al., 2005). The Y-shape junction was chosen because it was found that the system reached steady state bubble production faster and produced more stable bubbles in the liquid than the T-shaped junction.

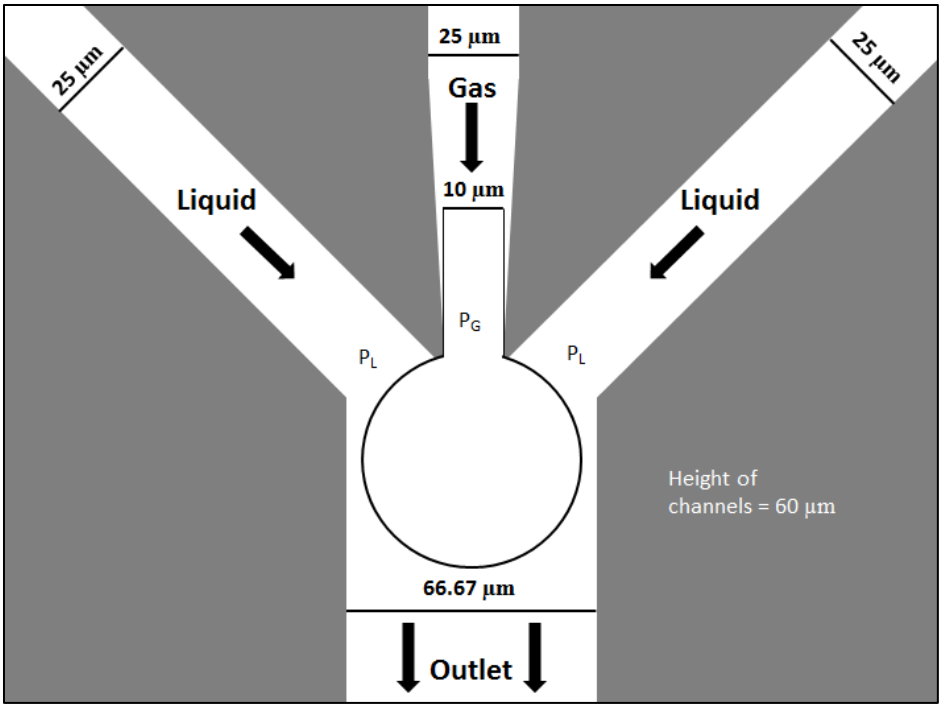

Figure 15. Design and size specifications of the Y-junction of the microfluidic device. The inlet channels for the liquid and the gas are 25 µm and the gas channel tapers to 10 µm at the junction which forms at a 40° angle. The outlet channel is 66.67 µm. Bubbles form in the junction, cutting off flow from the liquid channels except for a thin, wetting strip along the walls of the channel. The liquid pressure builds up and cuts off the bubble at the orifice. This process causes a cyclic bubble generation. All channels had a height of 60 µm.

In the microfluidic device, both liquid and gas are driven into the channels using an externally applied pressure gradient at near identical pressures. The liquid enters through the top inlet port and splits into two symmetric side channels. These two liquid channels combine, at a 40° angle, with a central gas channel, which tapers from 25 to 10 µm at the junction (Figure 3 and Figure 15). Bubbles are generated using hydrodynamic flow focusing; the gas stream is focused into an orifice using two side channel fluid flows. Upon entry, the gas stream is hydrodynamically pinched to create a steady stream of monodisperse gas bubbles. The dimensions of this device were experimentally optimized so each individual bubble displaces the two liquid streams at the junction, temporarily cutting off fluid flow except for a thin wetting stream along the walls of the outlet

channel. The wetting stream prevents the bubble from sticking to the sides of the channel and disrupting flow. As the bubble size and surface area increase, the influence of viscous drag from the two liquid streams eventually becomes larger than the interfacial forces holding the bubble at the nozzle, and the bubble detaches. When a continuous flow of liquid and gas are supplied, this process is repeated producing nearly identical bubbles at a constant frequency.

Bubble size can be controlled by adjusting the ratio of the liquid and gas stream flow rate through the external pressure applied to the microfluidic device. Increasing the gas pressure relative to the liquid pressure creates larger bubbles because more gas enters the bubble before the liquid stream pinches off the bubble and vice versa.

4.3 Bubble Sizes

The purpose of using the microfluidic bubbler was to create micro-scale bubbles to increase the mass transfer from gases to the bulk liquid. As a representative case study, air was bubbled through the liquid algae growth medium, BBM, using the microchannel set-up illustrated in Figure 3. For bubble flow, the pressure of the liquid and gas streams were set at similar pressures and then adjusted to facilitate bubble formation in the channels. Next, the size and distribution of bubble sizes produced in the liquid were evaluated. Shown in Figure 16A is an image of the bubbles produced by the microbubbler in the liquid while Figure 16B shows the bubbles produced from a typical industrial sparger, the device with the second smallest bubbles. Shown in Figure 17 is the size distribution of the bubbles produced by the microbubbler following multiple trials. The distribution shows that the bubbles from the microfluidic device averaged 114.41 microns in diameter at a flow rate of 0.50 mL/min.

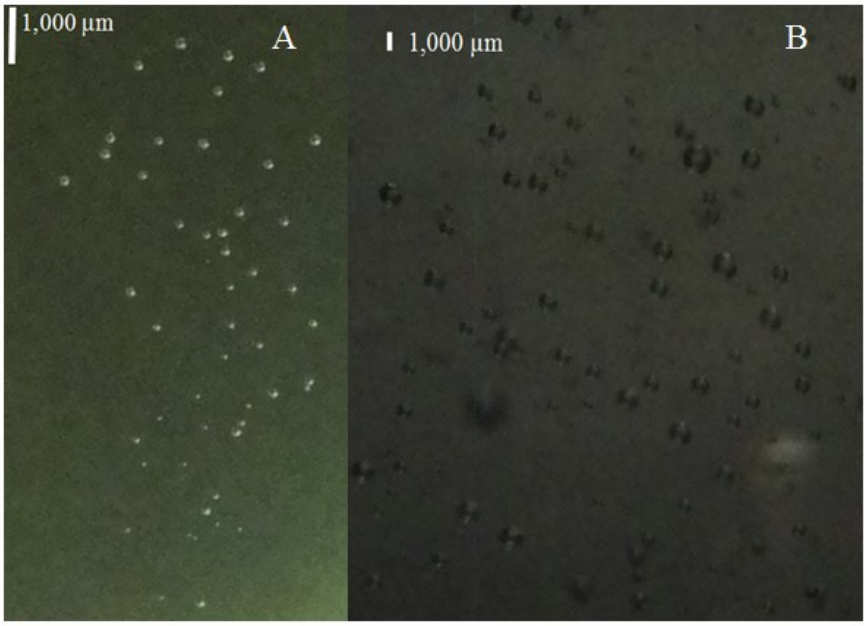

Figure 16. Bubbles formed in liquid media. Bubbles were generated by (A) the microfluidic bubbler at a flow rate of 0.50 mL/min and by (B) the next smallest alternative, the industrial sparger at 500 mL/min.

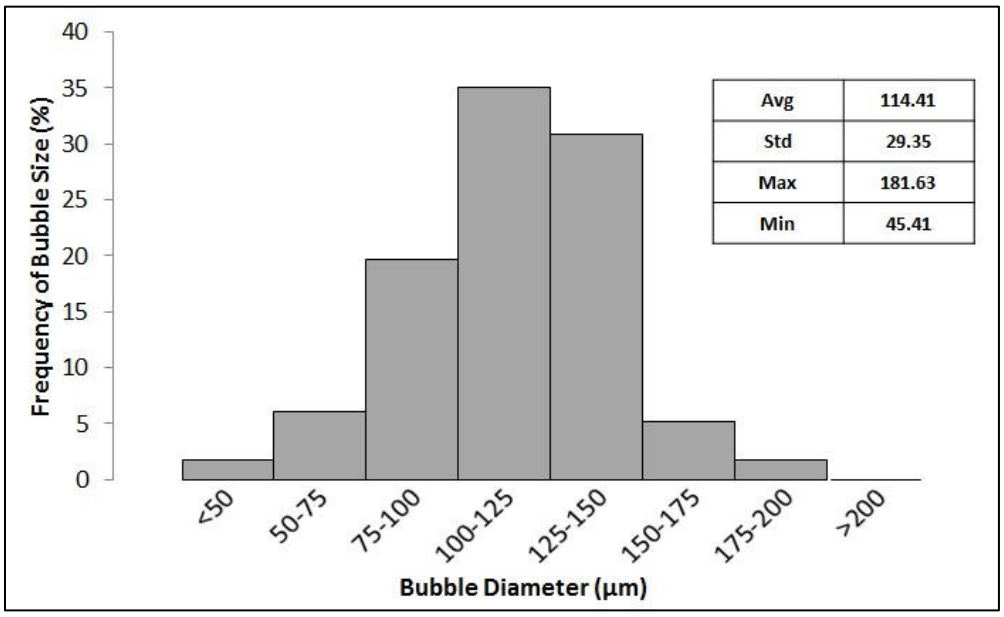

Figure 17. Size distribution of bubbles created by the microfluidic bubbler. The average bubble size for a flow rate of 0.50 mL/min was 114.41 µm with a standard deviation of 29.35 µm, a maximum size of 181.63 µm, and minimum size of 45.41 µm.

In order to see how the bubble size of the microfluidic bubbler compared to a range of other devices for supplying gas, the microfluidic device was compared to an open-tube, a

needle tip, an aquatic sparger, as well as an industrial sparger gas feeding system. Shown in Figure 18 is the average bubble size determined for the other four methods as a function of gas flow rate. Firstly, the microfluidic bubbler operates at a much lower flow rate than the other methods, with the other methods operating at minimum flow rates of 100, 400, 700, and 500 mL/min for the open-tube, needle, aquatic sparger, and industrial sparger, respectively. At lower flow rates, the other devices did not produce bubbles in the liquid media.

At extremely low flow rates, below ~1 mL/min, the bubbles of the microfluidic bubbler were all well below 1000 μm in diameter with the lowest average diameter of 114.41μm at a flow rate of 0.50 mL/min. The microfluidic device, needle, and open tube exhibit the requirement of trailing gas being pinched off to form bubbles, showing an increase in bubble size with flow rate (Du et al., 2002; Sayyaadi & Nematollahi, 2013). The bubble size stays relatively constant for both spargers based on their pore size, leading to the industrial sparger having slightly smaller bubble diameters due to more consistent, smaller diameter pores. The spargers created no bubbles below 500 and 700 mL/min for the industrial sparger and the aquatic sparger, respectively, due to too low of a pressure to push the gas through the pores.

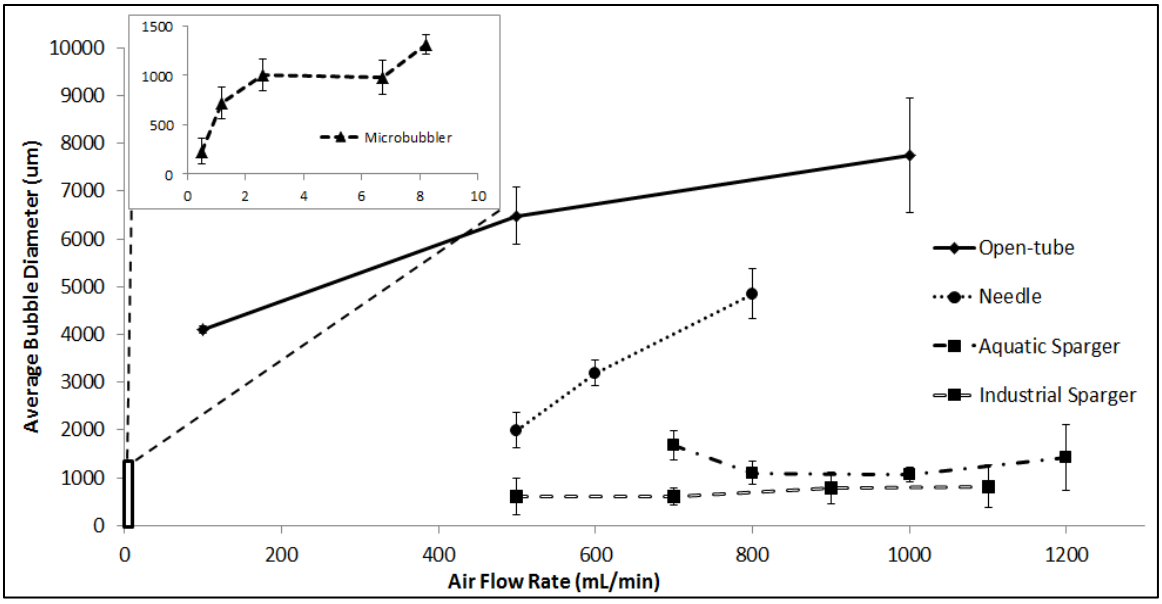

Figure 18. Bubble size dependence on flow rate for all devices. All bubble sizes increased with increasing flow rate except for both spargers, which remained constant. The microbubbler had the smallest bubbles, followed by the industrial sparger, aquatic sparger, the needle, and finally the open-tube.

4.4 K_La Determination

The goal of the microbubbler is to make gas solutes available in solution as effectively or more efficiently than conventional spargers. Therefore, the K_La was analyzed to see the mass transfer coefficient for the microbubbler, as shown in Figure 19A for the lower flow rates achieved. Interestingly, the K_La value for the microfluidic bubbler increased with increasing flow rate until 2.6 mL/min, corresponding to a K_La of 5.22 hr^{-1}. It has been shown, by others as well as these experimental results, that increasing flow rate increases K_La, shown in Figure 20 for the other common bubbling methods (Prasad & Ramanujam, 2009; Ying et al., 2013). After this peak, the K_La decreases gradually with increasing flow rate up to 8.2 mL/min, corresponding to a K_La of 4.16 hr^{-1}.

Because the flow rates of the systems were orders of magnitude apart and increasing flow rate increases K_La for most devices, the K_La values were normalized with flow rate and

the volume of the liquid tested (which remained constant), making this value dimensionless (Prasad & Ramanujam, 2009). Previous modelling studies have also normalized the K_La with the flow rate and volume (Badino Jr. et al., 2001). Shown in Figure 19B are the normalized K_La values for the microfluidic bubbler compared to the open-tube, needle, and sparger systems. According to the normalized K_La values, the microbubbler system is approximately 100 times more efficient in transferring mass from a gas to a liquid than the other aeration systems.

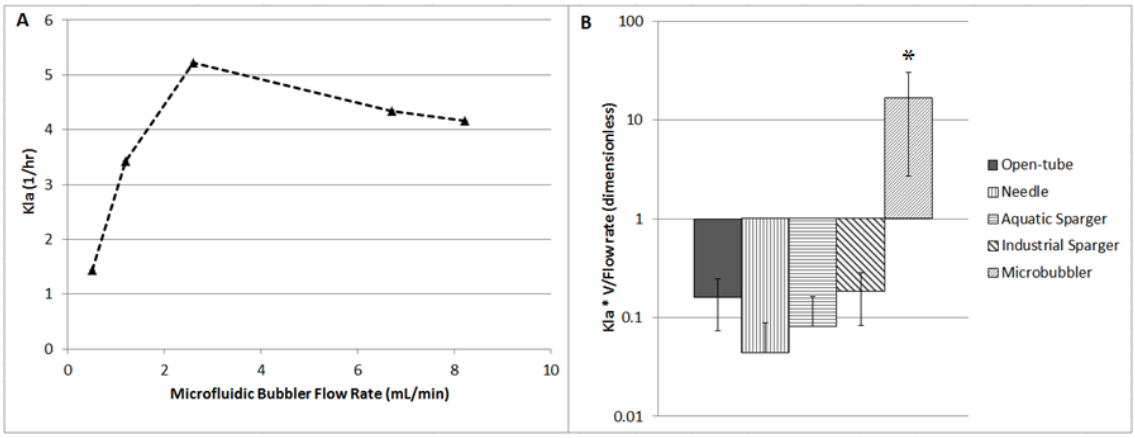

Figure 19. K_La and normalized K_La values for the microbubbler and other bubbling methods. (A) K_La dependence on flow rate for the microfluidic bubbler. K_La increased with flow rate until it peaked at 2.6 mL/min with a K_La of 5.22 hr^{-1}. At flow rates above the peak, the K_La decreased with increasing flow rate up to a maximum flow rate of 8.2 mL/min. (B) The K_La values for all systems were normalized with flow rate and volume of liquid, showing that the microfluidic device is two orders of magnitude better at transferring mass from a gas to a liquid. * indicates statistical significance with 95% certainty.

Lowering the flow rates of the other systems to create smaller bubbles and improve K_La values to compare to the microfluidic bubbler would not work for two reasons. The first comes from the fact that these other methods were operated at their lowest flow rate and lower flow rates will result in no bubbles. The other reason is that K_La decreased with decreasing flow rate, so decreasing the flow by two orders of magnitude would drop the K_La significantly (Figure 20).

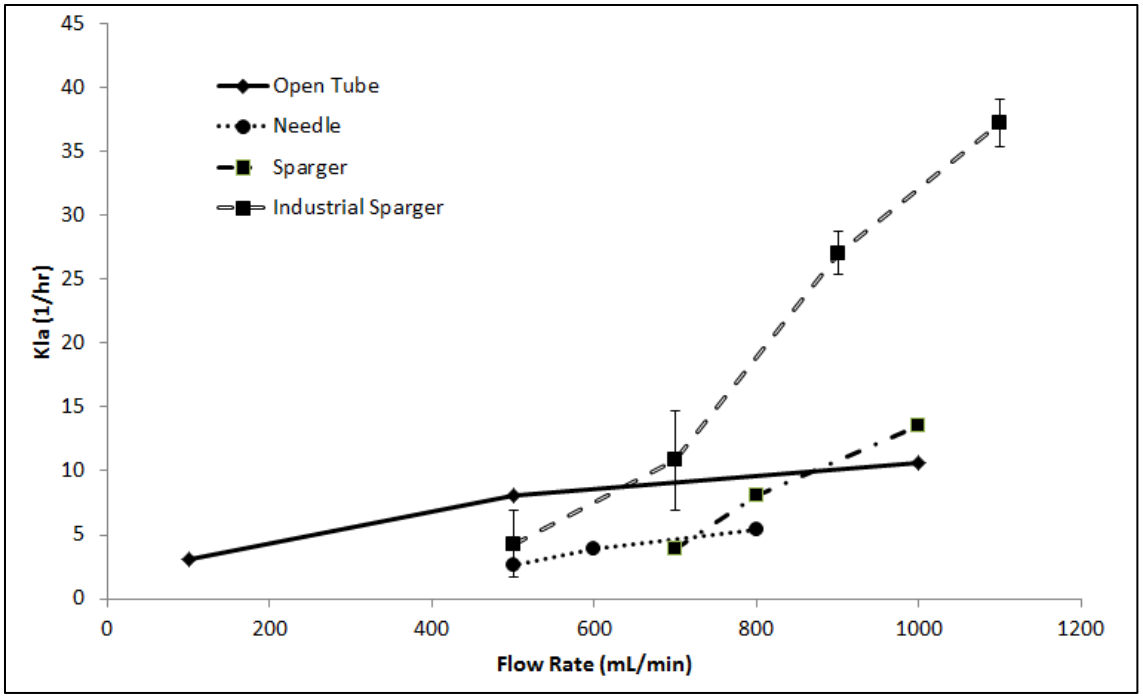

Figure 20. K_La dependence on flow rate for all devices. K_La increased with increasing flow rate for all devices with the industrial sparger having the highest K_La at high flow rates.

4.5 Fraction Transferred

In order to test how much of a particular solute is transferred from the microbubbles into solution, the fraction of oxygen transferred to the liquid (δ) was calculated by utilizing the K_La, C_a*, height (h) and cross sectional area (A_c) of the liquid, perpendicular to the flow, flow rate of the gas ($\dot{V}$), and the density of the gas (j) (Equation 8) (Al-Ahmady, 2006).

$$\delta = \frac{K_L a \cdot (C_a{}^*) \cdot h \cdot a_c}{\dot{V} \cdot J} \qquad \text{[Equation 8]}$$

Shown in Figure 21 are the values of fraction of oxygen transferred for different sparging devices. The fraction of oxygen transferred for the industrial sparger increases from 0.003 to 0.011 for flow rates of 500 to 1100 mL/min and the aquatic sparger increases from

0.002 to 0.005 for flow rates of 700 to 1000 mL/min. Conversely, the fraction transferred for the open-tube decreases from a maximum of 0.01 to 0.004 for flow rates from 100 to 1000 mL/min while the needle tip stays approximately constant at a fraction transferred of 0.002 for flow rates of 500 to 800 mL/min. In contrast, the microfluidic bubbler provides a significantly higher fraction of oxygen transferred of 0.91 and 0.90 at the lowest flow rates of 0.5 and 1.2 mL/min, respectively, indicating near complete transfer of oxygen.

Unlike the other devices, the fraction of oxygen transferred increases with decreasing flow rate for both the microfluidic bubbler and the open-tube device (Figure 21). Both the spargers increased the fraction of oxygen transferred with higher flow rates.

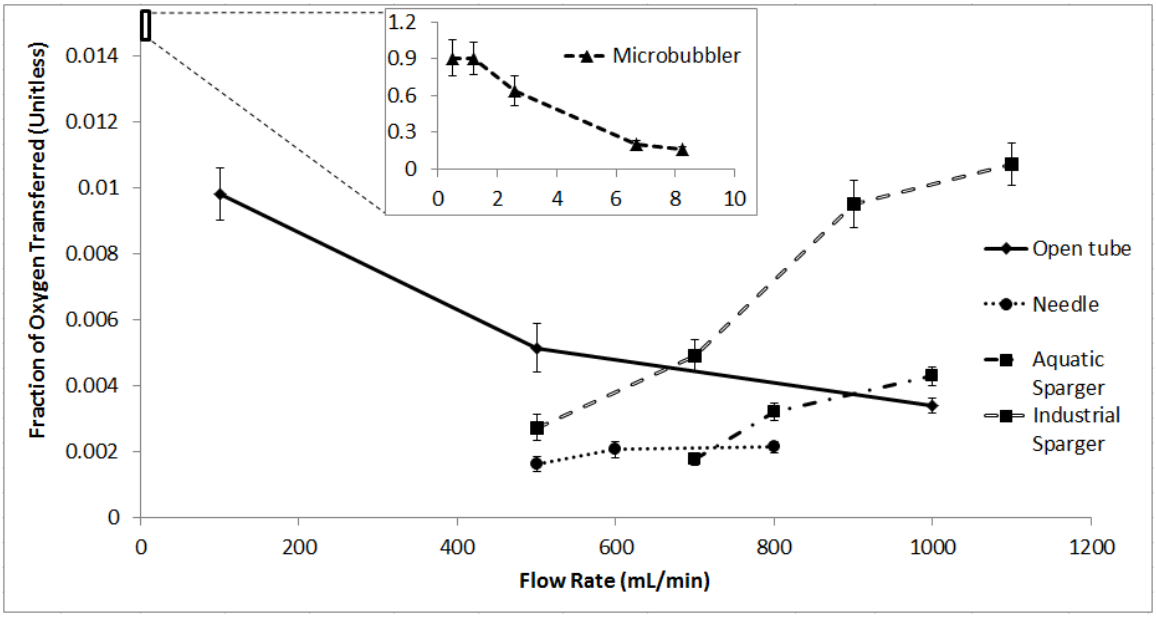

Figure 21. Fraction of oxygen transferred dependence on flow rate for all systems. For low flow rates (0.5 and 1.2 mL/min) of the microfluidic bubbler, the fraction oxygen transferred was approximately 0.90 while the fraction transferred for the other systems was generally less than 0.01.

This calculation utilizes information from the liquid to calculate the fraction of the gas transferred. As a secondary approach for evaluating the fraction of oxygen transferred,

the oxygen gas levels in the headspace were measured using an oxygen gas sensor throughout the K_La trials. The oxygen gas concentrations (C_O), the volume of the head space (V), and the flow rate (Q), can be used to calculate the concentration of oxygen in the bubbles leaving the liquid (G) using a modified dilution ventilation equation (Equation 9) (Wabeke, 1998).

$$\frac{dC}{dt} = \frac{Q \cdot (G - C_O)}{V} \qquad \text{[Equation 9]}$$

Integration of this equation can be used to calculate the concentration of oxygen in the outlet bubbles (Equation 10).

$$G = \frac{C_2 - C_1 \cdot e^{\left(\frac{-Q \cdot (t_2 - t_1)}{V}\right)}}{1 - e^{\left(\frac{-Q \cdot (t_2 - t_1)}{V}\right)}} \qquad \text{[Equation 10]}$$

The fraction of oxygen transferred using the off gas at any time t_2 can be calculated by dividing the concentration of oxygen in the outlet bubbles (G) by the concentration of oxygen in room air (209 parts per thousand (ppt)).

Shown in Figure 22 is the concentration of oxygen in the headspace for K_La testing of the microbubbler with a flow rate of 0.50 mL/min. The beginning of the oxygen transfer to the liquid (~17.5 minutes) began at the time at which nitrogen gas feeding was stopped and the microfluidic bubbler began flowing air into the media (see Section 2.5 K_La Determination). The oxygen gas concentration starts well below the concentration of oxygen in room air because nitrogen was previously fed to the system.

The oxygen level in the headspace progressively declined after the feed gas was switched to air fed via the microbubbler because of the transfer of oxygen from the air into the

liquid, leading to the replacement of oxygen with nitrogen and the other components of air, except oxygen, in the headspace. The bubbles, stripped of oxygen, led to a continual decline of oxygen concentration in the headspace. The concentration of oxygen in the bubbles was calculated based on a line of best fit for the change in concentration from the beginning to the end of the bubbling period, using Equation 10. Calculations indicated that the bubbles contained approximately 38.06 ppt oxygen, which corresponds to about 18% of oxygen in room air and a fraction of oxygen transferred of 0.82. Thus, the off gas fraction of oxygen transferred is similar in value to that calculated using Equation 8 (0.91), at an equivalent flow rate.

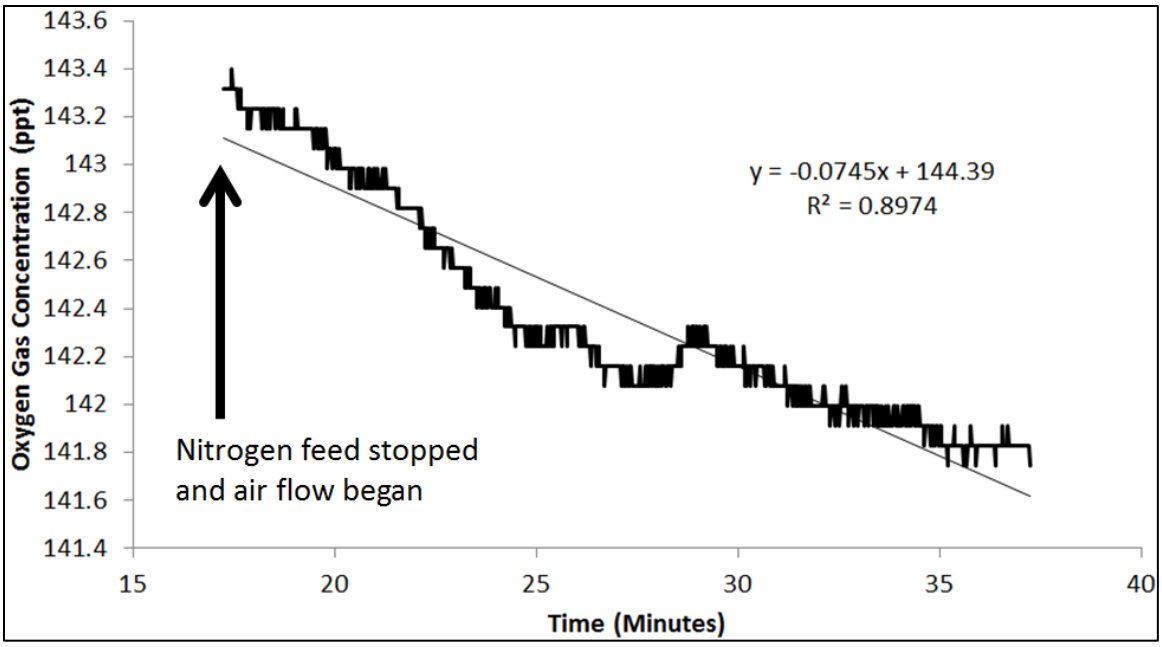

Figure 22. Oxygen gas concentration in the head space above the K_La testing. For a flow rate of 0.50 mL/min, the drop over time corresponded to a transfer of 82% of the oxygen in air to the liquid.

This system showed approximately 90% oxygen gas transfer to liquids at low flow rates from the dissolved oxygen calculation and around 82% from the oxygen gas calculations,

showing this high percentage of gas transferred was closely verified using two different methods.

4.6 Frequency Analysis

Once it was established that the microfluidic bubbler provided optimal conditions for transferring solutes from gas to a liquid, the frequency of bubble generation was measured over a range of liquid heights for various flow rates to see if it can be adjusted for larger reactor sizes (Figure 23). Below 30 cm in liquid height, the frequency of bubble generation stayed approximately constant at 2 to 18 bubbles per second for flow rates of 0.22 to 0.98 mL/min.

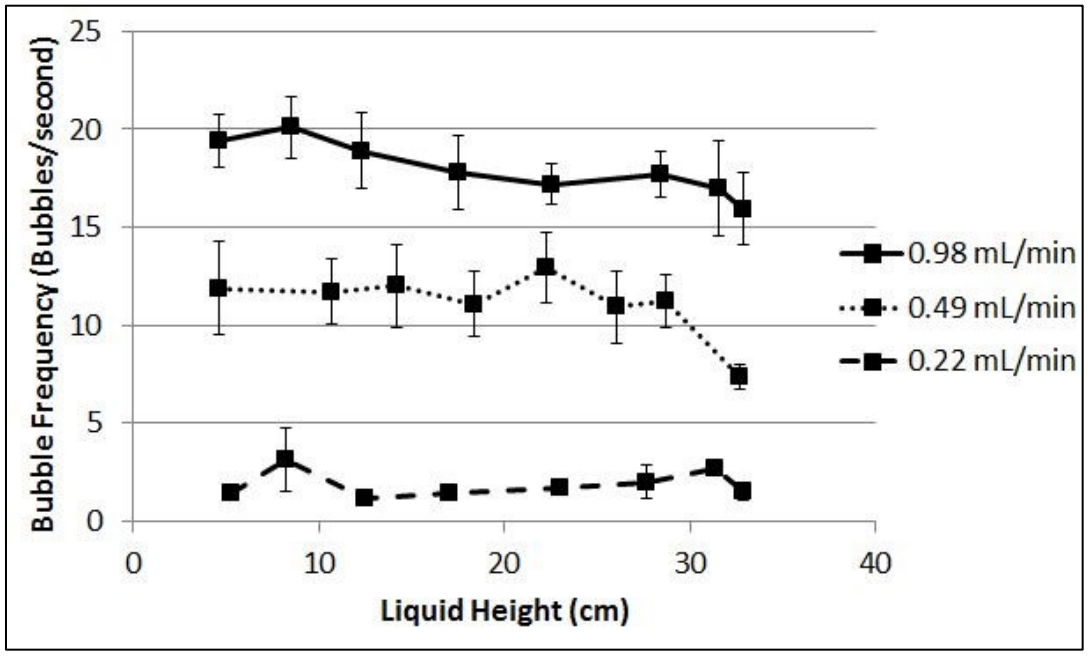

Figure 23. Bubble frequency dependence on height of liquid for a range of flow rates. Below 30 cm of liquid, the frequency stayed constant at approximately 2, 12, and 18 bubbles per second for 0.22, 0.49, and 0.98 mL/min, respectively.

The microbubbler can also work effectively at heights above 30 cm by increasing the pressure that drives the liquid and gas feeds. Increasing the flow rates also produces a

higher frequency of bubble generation, as verified by others as well as these results (Li et al., 1997; Olowson & Almstedt, 1990).

One aspect of the microbubblers that could pose a challenge for industrial use is that the pressure drop required for generating gas and liquid feed scales linearly with the device dimensions. In other words, a larger bubbler would require an equally larger pressure drop to produce the necessary bubble rate for industrial bioreactor use. These pressures could place new constraints on both the microfluidic device materials required to safely work under these pressures and the costs associated with continuously sustaining them in the bioreactor. While these devices can sustain 40 psi before the microfluidic channels rupture and debond from the glass substrate, future work will be needed to evaluate the feasibility of building devices at higher operating pressures as needed. Alternatively, smaller devices can be deployed in parallel and these permit generation of the small bubble sizes.

The flexibility of using different liquid operating heights provides a wide range of operating conditions and applications. For example, a microbubbler can be applied for bubbling gas to algal ponds in long raceways with shallow depths and bioreactors.

4.7 Bubbler Test in Culture

Next, the transfer of carbon dioxide, another sparingly soluble gas, was examined in growing algal cultures. The $K_L a$ value of carbon dioxide can be estimated by relating the measured $K_L a$ of oxygen in the system and applying the diffusivities of both gases, as described below in Equation 11 (Talbot et al., 1990).

$$K_L a(CO_2) = K_L a(O_2) \cdot \left(\frac{D_{CO_2}}{D_{O_2}}\right)^{0.5} \qquad \text{[Equation 11]}$$

A culture of *Chlorella vulgaris* was grown using the microbubbler and another culture with the needle tip using flow rates of 0.5 and 400 mL/min, respectively. The cells were grown for 240 hours and then growth and processing parameters were estimated and compared.

As shown in Figure 24, the culture with the needle tip at a flow rate two orders of magnitude higher exhibited a slightly higher growth rate and a final OD_{600} of 0.84 compared to 0.70 for the microbubbler. The difference corresponds to a biomass difference of 0.60 g/L for the needle tip versus 0.48 g/L for the microbubbler.

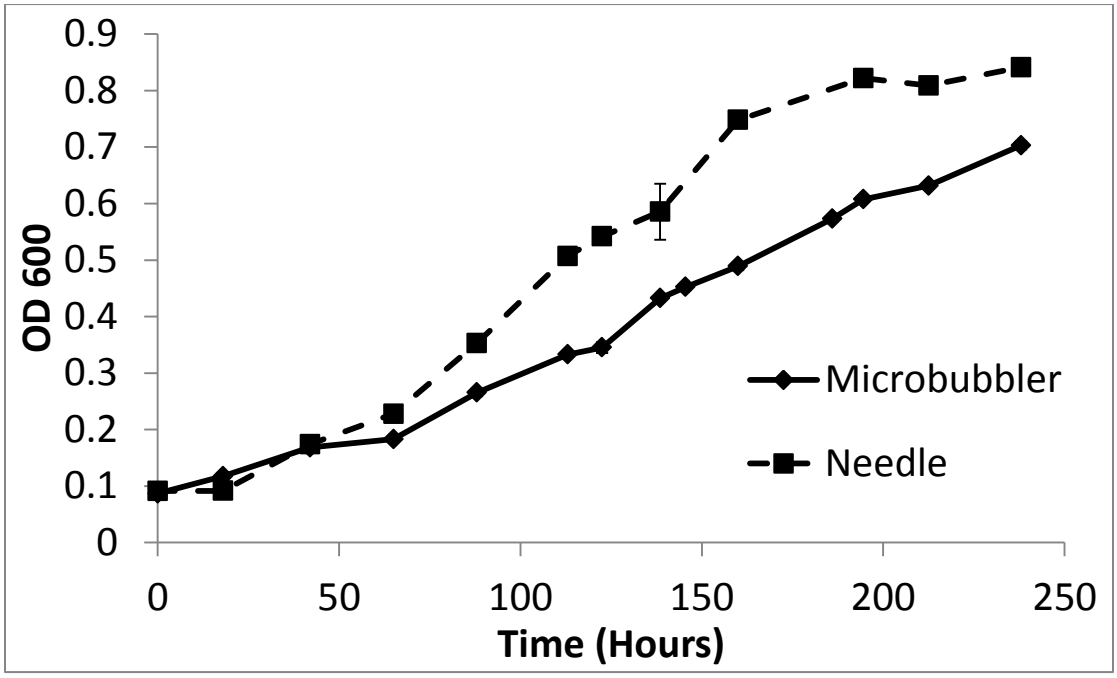

Figure 24. Growth curve for *Chlorella vulgaris* comparing the microbubbler to needle tip for gas feed. The needle culture (400 mL/min flow rate) grew slightly faster than the microbubbler culture (0.5 mL/min flow rate).

In addition to calculating the growth rates, the carbon dioxide concentrations in the headspace of the reactors were compared. As shown in Table 4, the carbon dioxide concentration in the headspace for the microbubbler culture was less than 10% of the

concentration of that in the headspace of the culture utilizing the needle tip. Furthermore, given that the feed gas contained 5,000 parts per million (ppm) CO_2, the microbubbler culture transferred more than 90% of the CO_2 in the feed. In contrast to this finding, the headspace for the needle feed had 98% of the feed gas concentration, meaning only 2% of the CO_2 in the feed gas was transferred to the culture. Overall, the total CO_2 fed per gram of biomass generated was 2.9 g for the microbubbler compared to 1900g for the needle tip, an almost 700 fold improvement.

Table 4. Flow and growth rates with CO_2 concentration in headspace and CO_2 fed per biomass for the microbubbler compared to needle bubbling. The 800 times lower flow rate of the microbubbler led to almost equivalent growth rates with a much lower carbon dioxide concentration in the headspace.

Bubbling Method	Flow Rate (mL/min)	Growth Rate (1/hr)	CO2 in Headspace (ppm)	CO2 Fed per Biomass (g CO2/g biomass)
Microbubbler	0.5 ± 0.1	0.015 ± 0.002	460 ± 100	2.9 ± 0.6
Needle	400 ± 20	0.018 ± 0.003	4900 ± 2500	1900 ± 100

The high fraction transferred of the microbubbler matched nearly identically to the calculations done for oxygen in previous sections. From the results, the microbubbler showed a much better fraction transferred and better overall growth and consumption of carbon dioxide in terms of total flow rate.

4.8 Economic Analysis

Another relevant consideration of the microfluidic bubblers is whether these devices are cost efficient for transferring solute at larger scales. As a first approximation, the cost of process inputs was compared for the devices based on the amount of mass transferred (Table 5). Input devices capital costs and additional costs due to pressure drops were ignored for this initial comparison but can be added in a more detailed comparison. In this analysis, the cost of media and gas needed per liter to run a typical microalgae

bioreactor with BBM media using 10% CO_2 in air at a required absorption rate of 162 mL of CO_2/minute/L culture were considered. An estimated required value of 162 mL of CO_2/min/L culture is calculated from the maximum theoretical photosynthetic rates of algal cultures using an estimated average cell density of $1x10^8$ cells/mL and ignoring shading effects (Lee & Palsson, 1994).

The amount of gas input was estimated given the the fraction of the gas transferred for each input system, since all systems, except the microbubbler, will require much higher flow rates to transfer a sufficient amount of gas for cellular consumption. As shown in Table 5, the processing costs per liter culture per time were nearly 4 times lower for the microbubbler when compared to the next most efficient systems, the open-tube and industrial sparger. Other systems, such as the needle and aquatic sparger, exhibit processing costs that were orders of magnitude higher due to the high amounts of CO_2 that must be pumped through these spargers to provide for sufficient dissolved CO_2 in the algal bioreactors.

Table 5. Economic analysis of the microbubbler system against other methods of bubbling. The analysis shows the cost of operation of the various gas sparging systems, showing the microbubbler has the lowest total cost.

System	Fraction Gas Transferred	Required CO2 Flow Rate (mL/min)	Total Cost/L culture/hour/fraction oxygen transferred ($/L/hr)
Microfluidic bubbler	0.908	178	1.76
Open tube	0.010	16532	7.56
Needle	0.002	75948	28.63
Aquatic Sparger	0.004	37767	15.09
Industrial Sparger	0.011	15139	7.07

However, final costs must also consider start-up costs of a microfabrication facility and costs associated with pumping the gases into the system. The implementation of a clean

room and equipment used for microfabrication include negative photoresists, developer solution, transparency mask, spin coater, mask aligner with ultraviolet (UV) lamp, and a tesla coil or oxygen plasma. The largest of these cost come from the costs for a clean room and a mask aligner with UV lamp. However, smaller, mobile clean rooms can be significantly less expensive, which can dramatically decrease the up-front manufacturing costs. However, once the equipment and clean room are in place, the cost of manufacturing the microfluidic bubblers is extremely low because the materials for making the devices (PDMS and cover slips) are inexpensive.

4.9 Microbubbler Conclusions

In this thesis, it was demonstrated that Y-junction microfluidic devices are able to form stable, small bubbles for use in transferring mass from gas bubbles to liquid. The small standard deviation on the bubble size distribution and the fact that 85% of the bubbles fall within a 75 μm span (75-150 μm), show that the microfluidic bubbler creates near constant bubble sizes at constant, low flow rates. The ability to accurately control and reproduce bubble sizes becomes increasingly important in processes in which it is important to reliably control all parameters, such as in complex biological processes or chemical reactions. This ability to fine-tune the sizes of the microbubbles will be especially critical for modelling and control purposes.

At low flow rates, the microfluidic bubbler generates bubbles much smaller (114.41 μm compared to >1000 μm) than the other systems, showing it outperforms the other system in creating small bubbles, especially at low flow rates. For the microfluidic bubbler, the open-tube, and the needle tip, the bubble diameter becomes larger with increasing flow

rate, as shown in Figure 18, consistent with findings from papers analyzing macroscopic bubble creation (Du et al., 2002; Sayyaadi & Nematollahi, 2013).

Another benefit to the microfluidic bubbler system is the low flow rates for operation of the microfluidic bubbler compared to the other methods of bubbling. The low flow rate of the microfluidic bubbler allows for a smaller amount of feed gas to form bubbles, which can generate significant savings for processes that use expensive gases. Because many processes, especially in the industrial setting, need a large gas flow rate, combining multiple devices in parallel will increase the total flow rate and improve the overall K_La further. Combining devices rather than adjusting the flow rate is a preferable option because raising the flow rate increases bubble diameter and lowers the efficiency of the transfer.

To verify that smaller bubbles improve mass transfer due to the larger surface area to volume ratio, the K_La was measured over a range of flow rates for the microfluidic bubbler. The K_La value for the microfluidic bubbler peaks at a flow rate of 2.6 mL/min. The peak occurs because as the flow rate starts to increase further, the bubble size increases. The larger bubble diameter gives the bubble a larger volume, increasing the buoyant force on the bubble, causing the faster rise velocity of the bubble (Talbot et al., 1990). This increased buoyant force causes the bubbles to rise out of the liquid faster, giving less time for transfer. Below the peak rate, the K_La decreases because less oxygen is released into the liquid, causing the dissolved oxygen concentration to not increase as rapidly, lowering the overall K_La (Badino Jr. et al., 2001; Sivasubramanian, 2010; Haribabu & Sivasubramanian, 2013). The standard deviations of the K_La values of the microbubbler stem from fast flow as the bubbles form and leave the output channel

followed by relatively slower flow rates while the bubbles form and push back on the liquid streams, lowering the gas flow rate. This cyclic fast/slow flow rates give rise to a higher standard deviation.

Comparing the microfluidic bubbler to the other devices in terms of the K_La normalized with flow rate demonstrates a 100 fold more efficient mass transfer for the microbubbler compared to other systems that have much higher flow rates. Using the microfluidic bubbler system, the most time efficient (highest K_La) system uses a flow rate of 2.6 mL/min, while the most complete transfer with the highest K_La per flow rate occurs at low flow rates of 0.5 mL/min.

The fraction of oxygen transferred decreases with increasing flow rate, similar to bubble size. The increased bubble size gives faster rise velocities and less time for the oxygen to transfer from the bubble to the liquid. At the lowest flow rates for the microfluidic device, the fraction of oxygen transferred is approximately 0.90, indicating almost complete transfer of the oxygen from the air to the liquid. This calculation was verified by analyzing the off-gas as part of the K_La measurements (Figure 22). By measuring the change in the headspace oxygen, the amount of oxygen transferred was estimated at 82%, which is similar to the value of 90% determined by Equation 8. More importantly, this high percentage of oxygen transfer shows the microfluidic bubbler improves gas mass transfer while minimizing the amount of feed gas necessary.

Although these results are significant advancements at the laboratory scale, it will be important to demonstrate scalability for larger vessels and in commercial application. This work has shown that this bubbler system at such low flow rates works extremely

well in volumes of liquid with heights up to 30 cm (Figure 23). It can also work effectively at heights above this by increasing the pressure that drives the liquid and gas feeds.

The frequency analysis revealed the large range of operating conditions and applications the bubbler can work at, such as in bioreactors. When implemented into an algal bioreactor, the microbubbler showed a much better fraction transferred and better overall growth and consumption of carbon dioxide than the needle tip in terms of total flow rate (Table 4). Obtaining nearly equivalent biomass with a flow rate 800 times lower demonstrates the substantial potential enhancements in mass transfer obtained using the microbubbler. Approximately 90% of the CO_2 was transferred in the microbubbler compared to only 2% for the needle tip approach, a 45 fold improvement in CO_2 transfer and utilization. The needle tip fed 1900g of CO_2 per gram of biomass whereas the microbubbler only fed 2.9g per gram of biomass, an almost 700 fold improvement.

Such an approach of using low flow rates with smaller bubbles for increased mass transfer can help provide significant cost savings by improving the efficiency of the transfer and limiting the amount of feed gas used (Table 5). From this analysis, the microfluidic bubbler is four times more cost efficient because of the lower requirement for feed gases. Furthermore, the savings of the microfluidic bubbler increase with larger systems and with extended use to suggest that this device will have value in a commercial setting.

The benefits of increased mass transfer due to low flow rates and small bubbles help make this microfluidic bubbler a more efficient method of bubbling gases through a

liquid. Carbon dioxide, oxygen, and other important gases, such as helium, can be sequestered from the gas phase by dissolving them into liquids more efficiently, providing environmental, cost, and efficiency benefits. The approach will allow users to harness and control gas delivery to liquids more effectively for a wide spectrum of engineering applications that could transform interfacial processes in the coming decades. A range of applications, varying from biochemical and biotechnological applications to chemical manufacturing, hydrometallurgy, and gas sequestration/recycling, can benefit from a complete redesign of bubbling systems to take advantage of the enormous benefits emerging from microfluidic technology advances.

Chapter 5
Summary and Future Work

5.1 Summary

The field of algae has exponentially grown over the past few decades. However, there is still a vast amount of research to be done in order to fully utilize this algae potential. Algae currently fix carbon dioxide and produce biofuels, nutraceuticals, proteins, and other useful products. All of these are currently costly and not a valid industrial option. With more research, algae culture costs will come down and can be used for industrial applications.

Cultures for one microalgae, *Chlorella vulgaris*, were tested under varying carbon dioxide levels to identify ideal gas flow rates to optimize growth and production of useful compounds. In terms of growth, biomass formation, lipid production, lutein production, and protein production, a 10% carbon dioxide feed to the cultures was ideal.

The 10% feed led to the largest productivity in terms of time and the cost of the feed gas for biomass, lipids, protein, chlorophyll, and lutein. All intracellular components had the highest concentration during the light cycles except for lutein, which increased in the dark to prevent oxidative damage from free radicals. These results led to the recommendation of a 10% CO_2 feed in continuous lighting for all intracellular components except for lutein, which should have a dark cycle at the end of the culture.

This 10% feed correlates to 80 mL of CO_2/min/L of culture. After analyzing the fraction of gases transferred using the needle tips used for these experiments, the fraction transferred was 0.002, corresponding to a usage of 0.16 mL of CO_2/min/L by the algae

cells. This flow rate of algae corresponds closely to theoretical calculations for the max photosynthetic rates of algae based on chlorophyll concentration and activity.

With so much of the gas wasted, a better system for transferring gas must be created. Therefore, a microfluidic device for generation of microbubbles was created. This microbubbler was able to create bubbles around 75-150 μm, more than 10 times smaller than other commonly used systems. The microbubbler also generated approximately equivalent K_La values to the other systems using 100 times lower flow rates, showing a 100 fold improvement in mass transfer per flow rate. The low flow rates and high K_La values lead to a fraction of gas transferred around 0.90, an almost 500 time improvement.

After showing the ability of the microbubbler to work in liquid heights up to 30 cm for macroscopic applications, the microbubbler was compared to a needle bubbler in algae cultures. The microbubbler improved the mass transfer rate of gas to liquid, improving the carbon dioxide consumption by algal cultures. At low flow rates, the microbubbler provided similar growth rates to other systems that use higher flow rates, showing it is applicable to macroscopic processes. The microbubbler culture used a flow rate 800 times lower with equivalent biomass, provided over 90% transfer of CO_2 compared to 2%, and fed only 2.9 g of CO_2 per gram of biomass compared to 1900 for the needle.

An economic analysis revealed the microbubbler to be four times more cost efficient than the open-tube and industrial sparger while being an order of magnitude better than the aquatic sparger and needle tip. The increased cost efficiency comes from having to feed less gas for the same amount of gas transferred.

The microbubbler can be used for other industrial applications to sequester gas, catalyze reactions, and many other processes. Furthermore, the microbubbler provide a significant advance in making algae cultures less expensive and a more viable method for biofuels, nutraceuticals, and other industrial applications by feeding the ideal amount of carbon dioxide.

5.2 Future Work

There is still much work to be done to continually improve the field of algae and make it a viable industrial option. The experiments to determine the optimal conditions for algae cultures should be repeated using the microbubbler to see how the increased gas transfer will affect the cultures. Smaller changes in the CO_2 feed should also be used to find the exact optimal conditions. Testing changes of 1% should elucidate the true ideal carbon dioxide feed conditions.

Increasing the concentration of CO_2 even further can provide insight on how CO_2 and pH inhibit growth and the concentration of CO_2 that will kill all cells. These concentrations can be tested with a more buffered system or with a pH control to see how higher CO_2 levels affect the cultures without the pH drops.

The free radical concentration should also be tested over time in the cultures to see how the carbon dioxide concentration in the feed gas affects their production. They should be tested to see if they are the cause of increased lutein production, which could lead to set culture conditions to induce lutein production.

Acclimating cells with lower CO_2 has already been found to allow cells to survive in extremely high carbon dioxide conditions (Yun et al., 1996). Testing the optimal way to

acclimate the cells could allow the cells to reach higher carbon dioxide concentrations, which could affect the production of lipids, proteins, pigments, etc. For all of the carbon dioxide experiments, the CO_2 gas in the head space should be analyzed to help determine the photosynthetic rates and optimal conditions.

With these repeated experiments, all of the intracellular components should be tested, such as carbohydrates, DNA/RNA, lipids, proteins, pigments, etc. Pigments, other than chlorophyll and lutein, should be investigated to see if other valuable carotenoids are made. All components should be tested as a time course throughout the culture as well to see how they change in the different stages of growth under varying carbon dioxide levels.

Another interesting experiment would be to feed small amounts of an organic carbon source, such as glucose, during the night cycles. This could prevent halts in growth and drops in cell weight during the dark cycles. These heterotrophic cycles could alter the percentages of intracellular components, such as lipids and lutein, and hopefully increase the desired products. The night cycle length could be altered to test the length at which cells start losing chlorophyll.

These experiments should also be scaled-up to show their applicability in an industrial setting. The scale-up should also look to incorporate the microbubbles. The microbubbler should be tested on a wide range of industrial applications to see if it is a viable option. If so, the microbubbler could make immediate improvements on these processes.

Once optimal feeds of carbon dioxide are found and are fed to the bioreactors with the microbubblers for high mass transfer, the limiting factor in photosynthesis will be the

cells. With enough light and carbon dioxide, the photosynthesis rates of the cells will limit the growth of the cells. Therefore, more enzymes, such as the ones involved in CO_2 uptake, photosynthesis, and the carbon capturing mechanism, can be added to the cells via plasmids to increase growth rates even further.

References

1. Al-Ahmady KK. (2006). Analysis of Oxygen Transfer Performance on Sub-surface Aeration Systems. International Journal of Environmental Research and Public Health, 3(3), 301-308.
2. Badino Jr. AC, Facciotti MCR, & Schmidell W. (2001). Volumetric oxygen transfer coefficients (K_La) in batch cultivations involving non-Newtonian broths. Biochemical Engineering Journal, 8, 111-119.
3. Ballantyne AP, Alden CB, Miller JB, Tans PP, & White JWC. (2012). Increase in observed net carbon dioxide uptake by land and oceans during the past 50 years. Nature, 408(7409), 70-72. doi: 10.1038/nature11299
4. Bischoff TR & Bold HC. (1963). Some soil algae from Enchanted Rock and related algal species. University of Texas Publications, No. 6022, 1-95.
5. Chelf P, Brown LM, & Wyman CE. (1992). Aquatic Biomass Resources and Carbon Dioxide Trapping. Biomass and Bioenergy, 4(3), 175-183.
6. Chen F & Johns MR. (1996). Relationship between substrate inhibition and maintenance energy of *Chlamydomonas reinhardtii* in heterotrophic culture. Journal of Applied Phycology, 8, 15-19.
7. Chinnasamy S, Ramakrishnan B, Bhatnagar A, & Das KC. (2009) Biomass Production Potential of a Wastewater Alga Chlorella vulgaris ARC 1 under Elevated Levels of CO2 and Temperature. International Journal of Molecular Sciences, 10, 518-532.
8. Clarens AF, Resurreccion EP, White MA, & Colosi LM. (2010). Environmental Life Cycle Comparison of Algae to Other Bioenergy Feedstocks. Environmental Science and Technology, 44, 1813-1819.
9. Del Camp JA & García-González M. (2007). Outdoor cultivation of microalgae for carotenoid production: current state and perspectives. Applied Microbiology and Biotechnology, 74, 1163-1174.
10. Dlugokencky E, & Tans P. (2015, March 5). *Global Greenhouse Gas Reference Network.* National Oceanic and Atmospheric Administration. Retrieved from http://www.esrl.noaa.gov/gmd/ccgg/trends/global.html
11. Drake BG & Gonzàlez-Meler MA. (1997). More Efficient Plants: A Consequence of Rising Atmospheric CO_2? Annual Review of Plant Physiology and Plant Molecular Biology, 48, 609-639.
12. Du L, Prokop A, & Tanner RD. (2002). Effect of bubble size on foam fractionation of ovalbumin. Applied Biochemisty and Biotechnology, 98-100, 1075-1091.
13. El-Sheekh MM, Bedaiwy MY, Osman ME, & Ismail MM. (2012). Mixotrophic and heterotrophic growth of some microalgae using extract of fungal-treated wheat bran. Journal of Recycling of Organic Waste in Agriculture, 1-12. doi: 10.1186/2251-7715-1-12
14. Estevez MS, Malanga G, & Puntarulo S. (2001). Iron-dependent oxidative stress in *Chlorella vulgaris*. Plant Science, 161, 9-17.
15. Garstecki P, Gañàn-Calvo AM, & Whitesides GM. (2005). Formation of bubbles and droplets in microfluidic systems. Bulletin of the Polish Academy of Sciences Technical Sciences, 53 (4), 361-372.
16. Gordillo FJL, Jiménez C, Figueroa FL, & Niell FX. (1999). Effects of increased atmospheric CO_2 and N supply on photosynthesis, growth and cell composition of the

cyanobacterium *Spirulina platensis* (*Arthrospira*). Journal of Applied Phycology, 10, 461-469.
17. Hallenbeck PC. (2012). Book. *Microbial Technologies in Advanced Biofuels Production*. New York City, New York: Spring US. doi: 10.1007/978-1-4614-1208-3
18. Hanotu, J., Hemaka Bandulasena, H. C., & Zimmerman, W. B. (2012). Microflotation Performance for Algal Separation. Biotechnology and Bioengineering, 109(7), 1663-1673.
19. Haribabu K & Sivasubramanian V. (2013). Determination of Mass Transfer Coefficients in an Inverse Fluidized Bed Reactor using Statistical and Dynamic Method for a Non-Newtonian Fluid. Journal of Scientific and Industrial Research, 72, 485-490.
20. Inskeep WP & Bloom PR. (1985). Extinction Coefficients of Chlorophyll a and b in N,N-Dimethylformamide and 80% Acetone. Plant Physiology, 77, 483-485.
21. Kadam KL. (2002). Environmental implications of power generation via col-microalgae cofiring. Energy, 27, 905-922.
22. Lee CG & Palsson BO. (1994). High-Density Algal Photobioreactors Using Light-Emitting Diodes. Biotechnology and Bioengineering, 44, 1161-1167.
23. Li QY, Cui ZF, & Pepper DS. (1997). Effect of bubble size and frequency on the permeate flux of gas sparged ultrafiltration with tubular membranes. Chemical Engineering Journal, 67(1), 71-75. doi: 10.1016/S1385-8947(97)00016-8
24. Lv JM, Cheng LH, Xu XH, Zhang L, & Chen HL. (2010). Enhanced lipid production of *Chlorella vulgaris* by adjustment of cultivation conditions. Bioresource Technology, 101, 6797-6804.
25. Martinez, C.J. (2009). Bubble generation in microfluidic devices. *Bubble Sci. Eng. Technol*., **1**(1), 40-51.
26. Murhammer DW & Goochee CF. (1988). Scaleup of Insect Cell Cultures: Protective Effects of Pluronic F-68. Nature Biotechnology, 6, 1411-1418. doi: 10.1038/nbt1288-1411
27. Olowson PA & Almstedt AE. (1990). Influence of pressure and fluidization velocity on the bubble behaviour and gas flow distribution in a fluidized bed. Chemical Engineering Science, 45(7), 1733-1741. doi: 10.1016/0009-2509(90)87051-S
28. Packer M. (2009). Algal capture of carbon dioxide; biomass generation as a tool for greenhouse gas mitigation with reference to New Zealand energy strategy and policy. Energy Policy, 37(8), 3428-3437.
29. Prasad KY & Ramanujam TK. (2009). Gas Holdup and Overall Volumetric Mass Transfer Coefficient in a Modified Reversed Flow Jet Loop Reactor. Canadian Journal of Chemical Engineering, 73(2), 190-195.
30. Prommuak C, Pavasant P, Quitain AT, Goto M, & Shotipruk A. (2012). Simultaneous Production of Biodiesel and Free Lutein from *Chlorella vulgaris*. Chemical Engineering Technology, 36(5), 733-739.
31. Rosenberg JN, Oyler GA, Wilkinson L, & Betenbaugh MJ. (2008). A green light for engineered algae: redirecting metabolism to fuel a biotechnology revolution. Current Opinion in Biotechnology, 19(5), 430-436.
32. Sayyaadi H & Nematollahi M. (2013). Determination of optimum injection flow rate to achieve maximum micro bubble drag reduction in ships; an experimental approach. Scientia Iranica, 20(3), 535-541.

33. Shah YT, Kelkar BG, & Godbole SP. (1982). Design Parameters Estimations for Bubble Column Reactors. AIChE Journal, 28 (3), 353-379. doi: 10.1002/aic.690280302
34. Sheehan J, Dunahay T, Benemann J, & Roessler P. A Look Back at the U.S. Department of Energy Aquatic Species Program: Biodiesel from Algae. National Renewable Energy Laboratory: Golden, CO, July 1998.
35. Sivasubramanian V. (2010). Gas-liquid mass transfer in three-phase inverse fluidized bed reactor with Newtonian and non-Newtonian fluids. Asia-Pacific Journal of Chemical Engineering, 5, 361-368. doi: 10.1002/apj.290
36. Talbot P, Gortares MP, Lencki RW, & de la Noüe J. (1990). Absorption of CO_2 in Algal Mass Culture Systems: A Different Characterization Approach. Biotechnology and Bioengineering, 37, 834-842.
37. Ting YP, Lawson F, & Prince IG. (1991). Uptake of Cadmium and Zinc by the Alga *Chlorella vulgaris*: II. Multi-ion Situation. Biotechnology and Bioengineering, 37, 445-455.
38. Veselá A & Wilhelm J. (2002). The Role of Carbon Dioxide in Free Radical Reactions of the Organism. Physiological Research, 51, 335-339.
39. Wabeke, R.L. Book. 1998. Air Contaminants and Industrial Hygiene Ventilation: A Handbook of Practical Calculations, Problems, and Solutions. Boca Raton (FL): Taylor and Francis.
40. Whitman, W. G. (1962). The Two-Film Theory of Gas Absorption. International Journal of Heat and Mass Transfer, 5, 429-433.
41. Widjaja A, Chien CC, & Ju YH. (2009). Study of increasing lipid production from fresh water microalgae *Chlorella vulgaris*. Journal of the Taiwan Institute of Chemical Engineers, 40, 13-20.
42. Yan H & Pan G. (2002). Toxicity and bioaccumulation of copper in three green microalgal species. Chemosphere, 49, 471-476.
43. Ying K, Al-Mashhadani MKH, Hanotu JO, Gilmour DJ, & Zimmerman WB. (2013). Enhanced Mass Transfer in Microbubble Driven Airlift Bioreactor for Microalgal Culture. Engineering, 5, 735-743. doi: 10.4236/eng.2013.59088
44. Yun YS, Park JM, & Yang JW. (1996). Enhancement of CO_2 Tolerance of *Chlorella vulgaris* by Gradual Increase of CO_2 Concentration. Biotechnology Techniques, 10(9), 713-716.
45. Zhang Z, Al-Rubeai M, & Thomas CR. (1992). Effect of Pluronic F-68 on the mechanical properties of mammalian cells. Enzyme and Microbial Technology, 14(12), 980-983. doi: 10.1016/0141-0229(92)90081-X

Biographical Statement

Jordan Baker was born on October 23, 1991 in Dover, Pennsylvania. He grew up and went to kindergarten through high school in Pottstown, Pennsylvania, eventually graduating as salutatorian from Owen J. Roberts High School. After high school, he attended Johns Hopkins University where he majored in chemical and biomolecular engineering with a concentration in molecular and cellular bioengineering. Jordan joined the research lab of Dr. Michael Betenbaugh at the end of his first year, beginning his research into algae as an alternative source for biofuels and other products. Jordan took a semester off in the fall of his senior year to complete a co-op at Genentech in San Francisco, California. After returning from the co-op, Jordan completed the five year program at Johns Hopkins University which consisted of a Bachelor's of Science and a Master's of Science in Engineering. Throughout the five years at Johns Hopkins University, Jordan performed research in the same lab of Dr. Betenbaugh which led to the research performed and presented here.